© 2016. Published by The Company of Biologists Ltd | Journal of Cell Science (2016) 129, 1734-1749 doi:10.1242/jcs.174920

TOOLS AND TECHNIQUES

A novel high-content analysis tool reveals Rab8-driven cytoskeletal reorganization through Rho GTPases, calpain and MT1-MMP

José J. Bravo-Cordero[1,*,‡], Marco Cordani[2,‡], Silvia F. Soriano[3,‡], Begoña Díez[2], Carmen Muñoz-Agudo[2], María Casanova-Acebes[2], César Boullosa[4], Marta C. Guadamillas[3], Iakes Ezkurdia[4], David González-Pisano[4], Miguel A. del Pozo[3] and María C. Montoya[2,§]

ABSTRACT

Rab8 is a small Ras-related GTPase that regulates polarized membrane transport to the plasma membrane. Here, we developed a high-content analysis (HCA) tool to dissect Rab8-mediated actin and focal adhesion reorganization that revealed that Rab8 activation significantly induced Rac1 and Tiam1 to mediate cortical actin polymerization and RhoA-dependent stress fibre disassembly. Rab8 activation increased Rac1 activity, whereas its depletion activated RhoA, which led to reorganization of the actin cytoskeleton. Rab8 was also associated with focal adhesions, promoting their disassembly in a microtubule-dependent manner. This Rab8 effect involved calpain, MT1-MMP (also known as MMP14) and Rho GTPases. Moreover, we demonstrate the role of Rab8 in the cell migration process. Indeed, Rab8 is required for EGF-induced cell polarization and chemotaxis, as well as for the directional persistency of intrinsic cell motility. These data reveal that Rab8 drives cell motility by mechanisms both dependent and independent of Rho GTPases, thereby regulating the establishment of cell polarity, turnover of focal adhesions and actin cytoskeleton rearrangements, thus determining the directionality of cell migration.

KEY WORDS: Actin, Cytoskeleton, Focal adhesion, Rab8, Rho GTPases, Migration, Proteases

INTRODUCTION

Cell migration is a biological process that contributes crucially to a variety of physiological events and allows tumour cells to invade surrounding tissues and generate metastasis. Membrane trafficking buffers the tension of the plasma membrane and maintains a polarized distribution of plasma membrane structural lipids and/or proteins, contributing to the extension of the plasma membrane at the protrusive front of the cell, and to the turnover of adhesions and retraction of the trailing edge (Bisi et al., 2013; Gauthier et al., 2012). Endocytic and exocytic trafficking are enriched at the leading edge (Hopkins et al., 1994; Howes et al., 2010; Schmoranzer et al., 2003) and at focal adhesions (Efimov and Kaverina, 2009; Ezratty et al., 2005; Stehbens et al., 2014). Interestingly, biosynthetic and recycling traffic of proteins from the trans-Golgi network to the plasma membrane is required for cell locomotion (Prigozhina and Waterman-Storer, 2006). Moreover, recycling of integrins to the front of migrating cells maintains their proper function at the cell surface during cell motility (Arjonen et al., 2012; Caswell et al., 2008; Powelka et al., 2004; White et al., 2007), and the trafficking of metalloproteinases, such as MT1-MMP regulates tumour cell invasion (Bravo-cordero et al., 2007; Steffen et al., 2008; Wiesner et al., 2013; Williams and Coppolino, 2011).

The Rho family of small GTPases are key elements controlling the actin cytoskeletal dynamics involved in cell migration. Rac1 induces actin polymerization at the lamellipodia and membrane ruffles, and the recruitment of cytoskeletal and signalling proteins into nascent focal complexes, whereas RhoA triggers actin stress fibre formation and induces the maturation of focal complexes into focal adhesions (reviewed in Hall, 2012). Rac1 and RhoA are modulators of cell migration, determining whether the cell has an intrinsic pattern of migration that is directionally persistent or randomly exploratory (Pankov et al., 2005). Several Rho family members are localized to intracellular vesicular compartments, and play important roles in membrane trafficking (reviewed in Bisi et al., 2013). There is also evidence indicating that membrane traffic regulates the activity of Rho GTPases, including Cdc42, which is regulated by the Rab8 and Rab11 recycling pathway (Bryant et al., 2010; Osmani et al., 2010), and Rac1, which is subject to Rab5-dependent endocytic trafficking (Palamidessi et al., 2008). Rab GTPases regulate budding, transport, tethering and fusion of vesicles, thereby providing specificity to membrane trafficking. Rab8-mediated traffic to the plasma membrane has been classically related to the secretory exocytic pathway (Henry and Sheff, 2008; Huber et al., 1993; Peränen et al., 1996), although it is also involved in the slow recycling route (Ang et al., 2003; Hattula et al., 2006; Roland et al., 2007; Yamamura et al., 2008). Rab8 is known to regulate polarized vesicle transport to the plasma membrane, and to promote actin and microtubule cytoskeletal rearrangements to mediate protrusion formation (Hattula et al., 2002; Huber et al., 1993; Peränen et al., 1996). In this study, we aimed to dissect the mechanism by which Rab8 regulates the organization of the cytoskeleton and to test whether it is involved in the migratory process.

The complexity of cytoskeletal rearrangements occurring during cell migration (focal adhesions, actin, etc.), their functional interdependence and the fact that they are subject to subcellular-location-specific regulation make the study of this process difficult.

[1]Confocal Microscopy Unit, Biotechnology Programme, Spanish National Cancer Research Centre (CNIO), C/Melchor Fernéndez Almagro 3, Madrid E28029, Spain. [2]Cellomics Unit, Cell Biology & Physiology Program, Cell & Developmental Biology Area, Centro Nacional de Investigaciones Cardiovasculares CNIC, C/ Melchor Fernandez Almagro 3, Madrid E28029, Spain. [3]Integrin Signaling Laboratory, Cell Biology & Physiology Program, Cell & Developmental Biology Area, Centro Nacional de Investigaciones Cardiovasculares Carlos III (CNIC), Melchor Fernández Almagro 3, Madrid E28029, Spain. [4]Structural Biology and Biocomputing Programme, Spanish National Cancer Research Centre (CNIO), C/Melchor Fernández Almagro 3, Madrid E28029, Spain.
*Present address: Division of Hematology and Oncology, Department of Medicine, Mount Sinai School of Medicine, Tisch Cancer Institute, New York, NY 1079, USA.
‡These authors contributed equally to this work

§Author for correspondence (mmontoya@cnic.es)

Received 27 May 2015; Accepted 29 February 2016

Journal of Cell Science

Journal of Cell Science (2016) 129, 1734-1749 doi:10.1242/jcs.174920

High-resolution analytical imaging techniques applied in large cellular populations are needed to analyse subcellular compartments after activation or inhibition of specific pathways in order to identify molecular mechanisms underlying different cell phenotypes. To achieve this goal, we developed a high-content analysis (HCA) tool that extracts quantitative measurements of actin and focal adhesions organization at subcellular resolution, and uses quantitative parameters to establish cytoskeletal rearrangement signatures, enabling us to explore the mechanism of Rab8-mediated cytoskeletal rearrangements. We found that Rab8 can induce Rac1- and Tiam1-dependent cortical actin polymerization and regulate microtubule-dependent focal adhesion disassembly through the proteases MT1-MMP (also known as MMP14) and calpain, and Rho-GTPase-dependent mechanisms. Moreover, we demonstrate that Rab8 is crucial for maintaining the directionality of the migrating cell.

RESULTS

Rab8 promotes actin cytoskeletal rearrangements and reorganization of focal adhesions as assessed by HCA

Rab8 has been reported to induce actin polymerization and protrusion, but the mechanism involved has not been studied in depth (Hattula et al., 2002, 2006; Peränen et al., 1996). To study how Rab8 overexpression and activation affect actin and focal adhesions organization, HeLa cells expressing the wild-type (WT; Rab8WT) or the constitutively active mutant of Rab8A (Rab8Q67L) were stained with phalloidin and vinculin and imaged by confocal microscopy. Expression of both Rab8 constructs (WT and Q67L) induced cortical cortical actin enrichment and loss of stress-fibre-like structures and focal adhesions (Fig. 1A). Interestingly, Rab8WT induced formation of multiple local actin-based cell protrusions, whereas the constitutively active Rab8Q67L mutant promoted widespread cortical actin rearrangements over the cell perimeter (Fig. 1A), suggesting that the promotion of cellular protrusions is dependent on Rab8 activation occurring locally at the cell surface.

To study the effect of Rab8 in cytoskeleton reorganization, we developed an HCA tool that quantifies cellular actin and focal adhesion re-organizations jointly in an automatic unbiased way by extracting quantitative measurements of both actin and focal adhesion organization from confocal fluorescence images of cells stained with phalloidin and vinculin. A segmentation scheme identifies individual cellular entities, which are classified based on GFP signal intensity to differentiate untransfected control cells from cells transiently transfected with GFP-tagged Rab8 constructs. Subsequently central (inner) and cortical (border) areas are identified based on the distance to the cell marginal border, segmenting actin (high intensity or fibrillar) and focal adhesion structures based on phalloidin and vinculin staining, respectively (Fig. 1B; Fig. S1). The software extracts quantitative features to measure actin and vinculin organization for each cellular entity, including descriptors of cortical actin, stress fibres, general actin, focal adhesion organization at the cell border (FAb) and inner (FAi) areas, or the whole-cell perimeter (FAc) which are numbered as indicated in Table S1. Analysis was performed in HeLa cells transfected with GFP, Rab8Q67L–GFP (Rab8Q), and Rab8WT–GFP (Rab8WT), in a transient manner because this allows comparison of GFP-expressing (GFP+, Rab8WT, Rab8Q) and non-expressing (GFP−) cells within the same sample and/or image for normalization purposes. Rab8 overexpression and activation induced cortical polymerized actin and decreased actin fibrillar structures in central (i.e. inner) areas of the cell (Fig. 1C–E). Accordingly, the balance between cortical (i.e. border) and central high intensity actin areas was affected drastically by Rab8 overexpression and activation (Fig. 1F). Rab8WT and Q67L expression reduced the area of small, medium and big focal adhesions, significantly lowering total, border and central relative focal adhesion areas, although focal adhesion reduction was more pronounced in central locations (Fig. 1G–L). Thus, Rab8 is involved not only in actin cytoskeleton organization – affecting both cortical actin and the formation of stress fibre – but also in the size and distribution of focal adhesions.

HCA-based identification of candidate molecular regulators of Rab8-promoted cytoskeletal rearrangements

Features obtained by HCA together determine a ‘phenotypic fingerprint’ combining the information of the different features that describe actin and focal adhesions to obtain a multiparametric cytoskeletal profile. Phenotypic profiles of HeLa cells transiently transfected with GFP, Rab8Q67L–GFP or Rab8WT–GFP were computed as a representation of phenotypic feature deviations obtained for GFP+ cells normalized to the GFP-negative population as described previously (Collinet et al., 2010). These profiles show the effect of Rab8-WT and -Q67L constructs on inducing cortical actin rearrangement and the distribution of focal adhesions at the cell border (positive deviations), while reducing stress fibre and focal adhesion relative areas (negative deviations) (Fig. 2A,B). Consistent with the expected absence of phenotypic effects, control GFP-expressing cells displayed negligible deviations from the GFP-negative population, thus yielding null values. Phenotypic profiling of Rab8WT–GFP-induced actin and focal adhesion reorganizations was studied in cells in which gene knockdown (KD) was achieved by prior reverse transfection with oligonucleotide small interfering RNAs (siRNAs). Fingerprints offer a holistic view of cytoskeletal rearrangements promoted by Rab8, and were therefore used to identify genes altering Rab8 induced cytoskeletal rearrangements. We tested a small set of siRNAs targeting genes related to actin and focal adhesion cytoskeletal reorganization [Rac1, Tiam1, Tiam2, calpain 1, calpain 2 and calpain 4 (also known as Capns1), MT1-MMP, and TRPM6 and TRPM7], Rab8 function (Ocrl and Cep290) and kinases with homology to known Rab8 effectors [TNIK, MINK (also known as MINK1) and HGK (also known as MAP4K4)]. Hierarchical clustering of the multiparametric profiles of cells in which the different genes had been silenced allowed us to identify genes based on their ability to induce similar perturbations to the Rab8-induced phenotype; the most remarkable differences were found for a cluster of the Capns1, Tiam1, MT1-MMP and TRPM7 genes, whereas Rac1 profiling also displayed important differences to control that deserved further studies (Fig. 2C; the raw data is available from the corresponding author upon request).

Rab8 regulates Rac1-, and Tiam1- and Tiam2-dependent cortical actin polymerization and RhoA-dependent stress fibre reorganization

We addressed the involvement of Rac1 GTPase, a key coordinator of cytoskeletal changes required for directional cell movement (Hall, 2012), in Rab8-mediated actin reorganization. Rac1 knockdown in Rab8WT-expressing cells consistently reduced the Rab8-mediated increase in cortical actin but had no effect on the reduction of stress fibres (Fig. 3A,B), indicating that Rac1 is responsible for Rab8-induced actin rearrangements in cell protrusions. Accordingly, expression of Rab8Q67L increased Rac1 activity as assessed by a pulldown assay (Fig. 3C) and FRET assays (Fig. S2F). Rac1 and its guanine-nucleotide-exchange factors (GEFs) Tiam1 and Tiam2 are involved in the regulation of

Journal of Cell Science (2016) 129, 1734-1749 doi:10.1242/jcs.174920

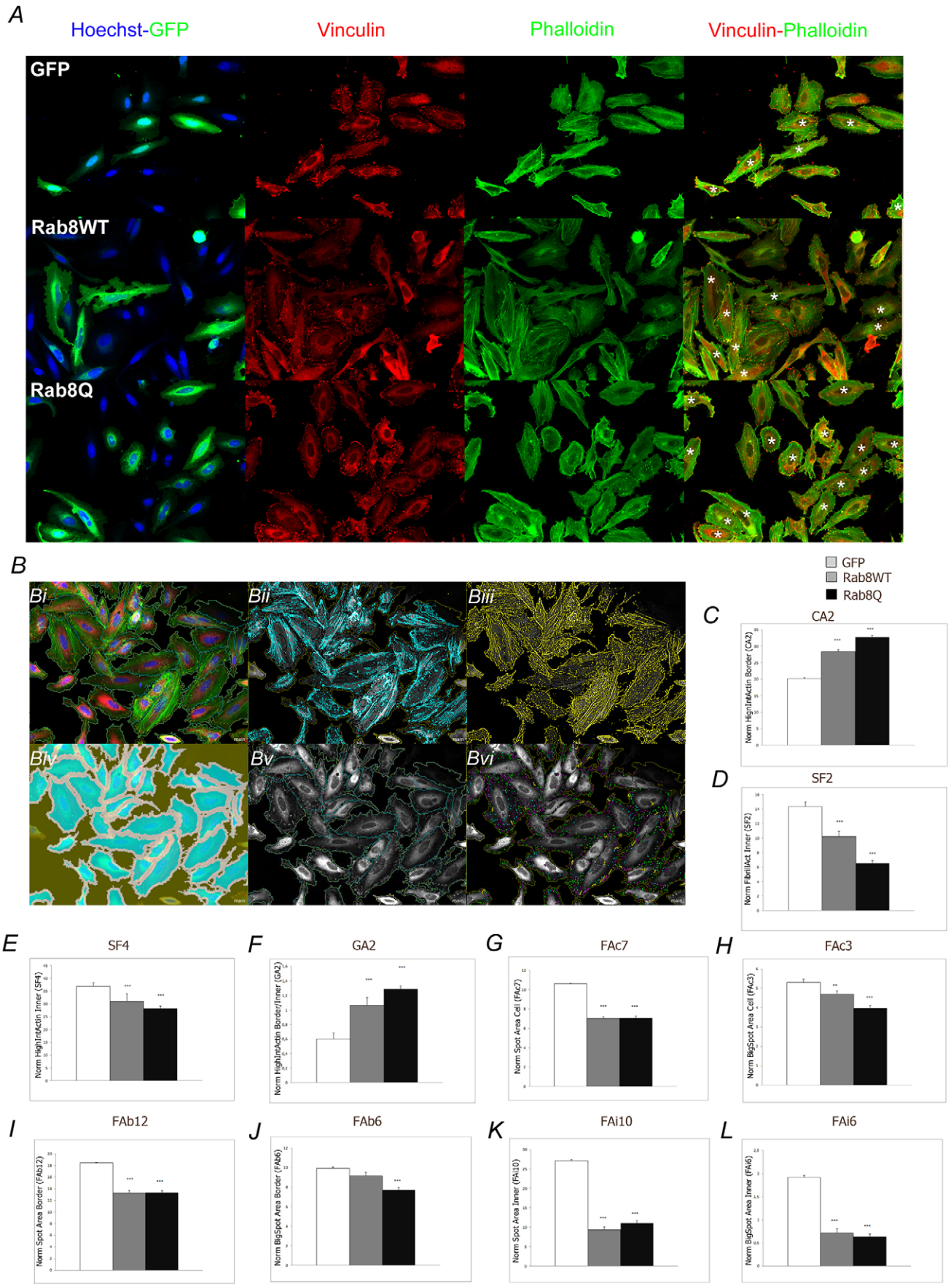

Fig. 1. See next page for legend.

Journal of Cell Science (2016) 129, 1734-1749 doi:10.1242/jcs.174920

Fig. 1. HCA of actin and focal adhesion rearrangements promoted by Rab8 overexpression and activation. HeLa cells transiently expressing GFP, Rab8Q67L–GFP (Rab8Q) or Rab8WT–GFP (Rab8WT) were plated on fibronectin (Fn), then fixed and stained with phalloidin or anti-vinculin antibody to reveal actin and focal adhesions. (A) Representative fluorescence confocal images showing overlay of GFP (green) and Hoechst 33342 (blue), single staining of vinculin (red) and phalloidin (green), and an overlay of vinculin and phalloidin staining, as indicated. Asterisks depict GFP-positive cells expressing the indicated constructs. (B) Representative fluorescence confocal images of HeLa cells stained as in A and associated image-processing segmentation results. (Bi) Overlay of phalloidin (green), vinculin (red) and Hoechst 33342 (blue) fluorescence confocal images and highlighted cell segmentation. (Bii,iii) Phalloidin staining and highlighted segmentation of (Bii) high-intensity actin (cyan) and (Biii) fibrillar actin structures (yellow). (Biv,vi) Vinculin staining and highlighted segmentation of (Biv) cell border and inner areas (white and blue, respectively), and (Bv) cell contours (blue) and (Bvi) focal adhesions (small, cyan; medium, green; and big, purple or yellow). (C–M) Graphic representations of cortical-actin-, stress-fibre- and focal-adhesion-related features quantified in HeLa cells treated as in A. Values represent mean±s.e.m. from individual cells expressing GFP (n=1012), Rab8WT (n=143) and Rab8Q (n=166) from a representative experiment out of five independent experiments. $^{**}P<0.01$; $^{***}P<0.001$ (between experimental and control values as evaluated by a two-tailed Mann–Whitney test).

the actin polymerization machinery that drives cell motility and in focal adhesion disassembly (Hamelers et al., 2005; Rooney et al., 2010). HCA profile analysis revealed that Rab8-mediated cortical actin polymerization was partially impaired by Rac1 or Tiam1 KD, but not by Tiam2 KD. In turn, stress fibre disassembly induced by Rab8 overexpression was only slightly compensated for by Rac1, Tiam1 or Tiam2 KD (Fig. 3A,B), suggesting that the Rac1 GEF Tiam1 is involved in the Rab8-induced cortical actin increase, but that alternative mechanisms are responsible for Rab8-induced stress fibre rearrangements. To explore the underlying mechanism, we stained endogenous Rab8 and Tiam1, which were found to colocalize at protrusive cortical membranes (Fig. 3D). Cells expressing exogenous GFP-tagged Rab8WT or Rab8Q67L revealed localization of Rab8 with endogenous Tiam1 in independent vesicular structures decorating microtubules and also colocalization at cortical membrane areas (Fig. 3E) suggesting they are localized at different vesicular compartments and converge at the plasma membrane. Interestingly, Tiam1 is mainly localized at intracellular storage compartments in confluent monolayers, which are greatly diminished by the expression of Rab8Q67L (Fig. 3F), suggesting that Rab8 promotes Tiam1 mobilization from intracellular compartments or their arrest at cortical locations. Rab8Q67L-induced cortical actin enrichment and loss of stress fibres were impaired by expression of constitutively active RhoA (RhoV14) (Fig. 3G–I), revealing that RhoA inhibition is involved in Rab8-induced Rac1-independent stress fibre rearrangements. Taken together, these results demonstrate that Rab8 activation induces Rac1 activity, which promotes cortical actin polymerization in a manner dependent on Rac1 and Tiam1 and independent of RhoA.

Rab8 promotes microtubule-driven RhoA, MT1-MMP and calpain-dependent focal adhesion loss

Cell migration involves the continuous formation and disassembly of adhesive structures (Etienne-Manneville, 2013; Stehbens and Wittmann, 2012). Our results indicate that changes in Rab8 expression and activation status dramatically affect focal adhesion area and distribution. Rab8 overexpression and activation promoted a reduction of focal adhesion area that was not completely restored by Rac1, Tiam1 or Tiam2 KD, which impaired reduction of border focal adhesions but only partially restored loss of inner focal adhesions (Figs 3A and 4A). Rac1 activation is thus involved in focal adhesion loss, most probably by antagonizing RhoA to generate a defect in cortical focal adhesion maturation. Coexpression of constitutively active mutants of RhoA or GEFH1 with Rab8 abolished border focal adhesion reduction elicited by Rab8 expression, but did not restore Rab8-promoted loss of inner focal adhesions (Fig. 4B,C), suggesting that RhoA-independent additional mechanisms are involved in the regulation of focal adhesions at cellular central areas.

Our results have shown that the matrix metalloproteinase MT1-MMP and the Ca^{2+}-dependent protease calpain are involved in Rab8-mediated cytoskeletal rearrangements (Fig. 2C). Given that both proteases have been implicated in focal adhesion disassembly (Franco et al., 2004; Takino et al., 2006; Wang and McNiven, 2012), we further explored their role in Rab8-promoted focal adhesion disassembly by targeting them with siRNAs or chemical inhibitors. As a control we used Cep290, a centrosomal protein that interacts with Rab8 in cilia, given that its KD has no effect on Rab8-promoted focal adhesion reorganizations (Fig. 2C). Knockdown of MT1-MMP or the small regulatory subunit of calpain (Capns1) partially rescued the loss of focal adhesions in the whole cell perimeter (FAc) and fully rescued the Rab8-promoted border focal adhesion area reduction. However, Rab8-dependent loss of focal adhesions from inner and central localizations was more pronounced when Capns1 was knocked down and was only partially restored by MT1-MMP KD (Fig. 4D,E), revealing that Rab8-regulated focal adhesion disassembly involves a complex interplay between MT1-MMP and calpain proteolytic activities. Furthermore, vesicular localization of both proteases was hampered by Rab8 KD, especially at cortical areas, and impaired proteolytic processing of talin, a calpain target at focal adhesions (Fig. S3A–D), suggesting a role of Rab8 in the traffic of these proteases to the plasma membrane. Analysis of focal adhesion organization was carried out in cells pre-treated with chemical inhibitors of metalloproteinases (GM110) and calpain (ALLM). The MMP inhibitor promoted a redistribution of focal adhesions to central areas, similar to that caused by the microtubule-disrupting agent nocodazole (Fig. 4F,G); however, in contrast to nocodazole treatment, GM110 inhibitor could not restore the Rab8-induced loss in these inner focal adhesions. In turn, the calpain inhibitor produced a massive increase in border focal adhesions, which were virtually absent from central cellular localizations and impaired the Rab8-promoted loss of border focal adhesions (Fig. 4F,G). Taken together these data suggest that calpain mediates cortical focal adhesion turnover and/or sliding towards the cell centre, whereas MMPs are involved in both turnover at the cell border and disassembly of focal adhesions from central areas of the cell body. The net effect of Rab8 overexpression on cellular focal adhesion area could not be impaired by any of these inhibitors alone, implying that both proteases act on different Rab8-dependent focal adhesion regulatory pathways. Nocodazole treatment, however, abolished Rab8-induced net focal adhesion loss, demonstrating the requirement for microtubules in this process.

Rab8 localizes dynamically to cellular protrusions and focal adhesions in carcinoma cells to promote actin rearrangements and focal adhesion disassembly

Having established the mechanism by which the expression and activation of Rab8 promotes cytoskeletal rearrangements, we evaluated the contribution of endogenous Rab8 in the metastatic breast carcinoma cell line MDA-MB-231 by knocking down its

Journal of Cell Science (2016) 129, 1734-1749 doi:10.1242/jcs.174920

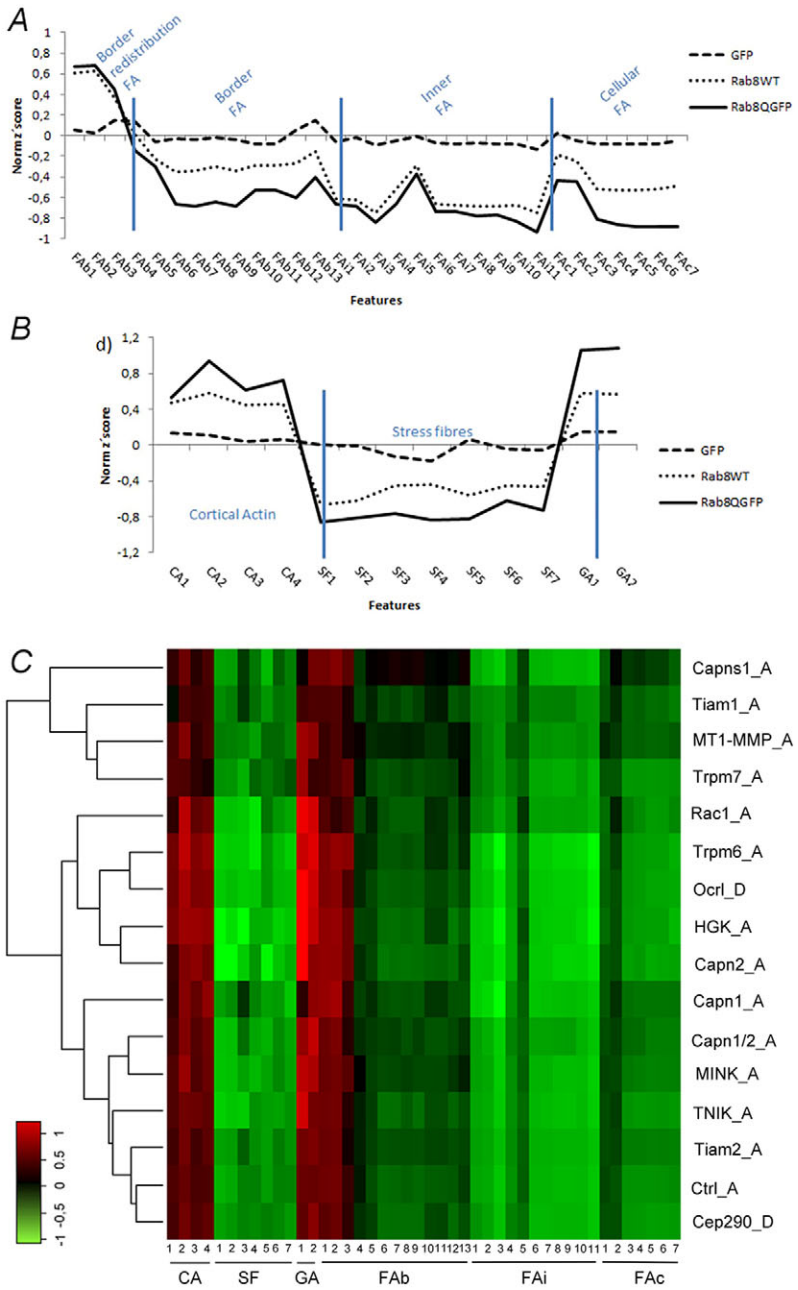

Fig. 2. Multiparametric cytoskeletal rearrangement profiling and resulting hierarchical clustering analysis of the effect of siRNAs on the Rab8WT phenotype. HeLa cells expressing GFP, Rab8WT–GFP or Rab8Q–GFP constructs were stained with phalloidin, anti-vinculin antibody and Hoechst 33342, and HCA was performed to extract phenotypic parameters, which are plotted as normalized *Z*-values describing the organization of (A) focal adhesions and (B) actin. (A) Focal adhesion rearrangement profile. Focal adhesion parameters are grouped as border focal adhesions (FAb), inner focal adhesions (FAi) and cellular focal adhesions (FAc). (B) Actin rearrangement profile obtained as described in the Materials and Methods. Parameters are grouped as cortical actin (CA), stress fibre (SF) or general actin organization (GA) descriptors. Values represent mean *Z*-scores and were obtained from a representative experiment out of five independent experiments in which individual cells expressing GFP, Rab8WT and Rab8Q were analysed (n=1008, 142 and 216, respectively). (C) HeLa cells were transfected with no targeting (Ctrl) or with siRNAs targeting the indicated genes (right) and then with Rab8WT–GFP. Cells were stained with phalloidin, anti-vinculin and Hoechst 33342 to extract phenotypic profiles of actin rearrangements by HCA. The heatmap shows unsupervised hierarchical clustering of profiles of the indicated parameters (bottom).

expression with short hairpin RNA (shRNA). Cells expressing non-targeting control (shCtrl) or Rab8A-targeting (shRab8) shRNA vectors were stained with phalloidin and vinculin and imaged by confocal microscopy. Rab8 KD significantly induced stress fibre assembly and reduced cortical actin levels, while promoting a reorganization of focal adhesions, which appeared larger and more abundant at central cellular areas (Fig. 5A). Although Rab8 shRNA did not induce a significant increase in the border focal adhesion area, the focal adhesions of both border and inner areas were significantly bigger (Fig. 5A,B). Ectopic expression of an mRFP-tagged Rab8 coding sequence carrying four silent mutations in the Rab8 shRNA target sequence, Rab8^{mut}, rescued the effects of Rab8 depletion, producing similar effects to Rab8Q67L expression in these cells (Fig. S2A). Expression of a constitutively active mutant in MDA-MB-231 cells promoted similar effects to those observed in HeLa cells, although they were less marked because these cells express high levels of Rab8 and accordingly display more prominent cortical actin polymerization and less evident stress fibres (Fig. S2C–E). Consistent with this, cortical actin induced by Rab8Q67L, but not stress fibre loss, was also impaired by previous KD of Rac1 in MDA-MB-231 cells (Fig. S2C–E), confirming that Rab8-mediated cortical actin polymerization is Rac1 dependent in this cellular model. Interestingly, Rab8 depletion increased RhoA activity (Fig. 5C) and stress fibre assembly (Fig. 5A,B). HCA revealed that the stress fibre increase promoted by Rab8 KD was impaired by RhoA siRNA whereas cortical actin reduction was not (Fig. 5D–F), indicating that the stress fibre increase promoted by Rab8 is RhoA dependent, whereas reduction of cortical actin is RhoA independent. Taken together, these results demonstrate that Rab8 KD increases RhoA activity and promotes Rac1-independent and RhoA-dependent stress fibre assembly.

Journal of Cell Science (2016) 129, 1734-1749 doi:10.1242/jcs.174920

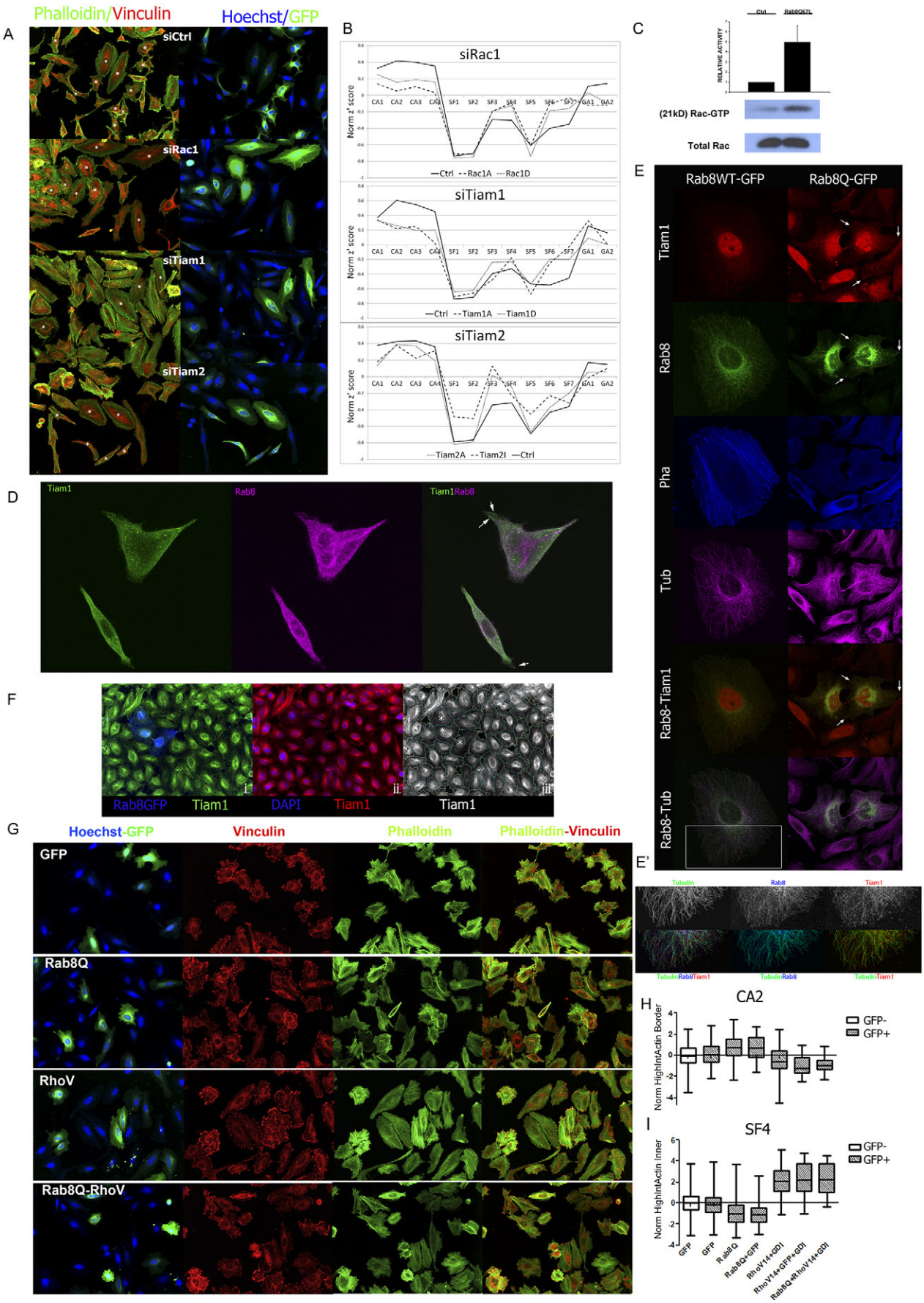

Fig. 3. See next page for legend.

Journal of Cell Science

Journal of Cell Science (2016) 129, 1734-1749 doi:10.1242/jcs.174920

Fig. 3. Rab8-promoted actin rearrangements are dependent on Rac1, Tiam1 and RhoA. (A,B) HeLa cells were transfected with siRNAs as indicated and then with Rab8WT–GFP. Cells were stained with phalloidin, anti-vinculin antibody and Hoechst 33342 to extract phenotypic profiles of actin rearrangements by HCA. (A) Representative images of Hoechst 33342 and GFP (overlaid, right), and phalloidin and vinculin (overlaid, left) in which Rab8GFP expressing cells are highlighted with asterisks. (B) Actin rearrangement profiles of cells transfected with the siRNAs targeting the indicated genes obtained by HCA as described in the Materials and Methods. Values represent mean *Z*-scores obtained from one representative experiment out of three independent experiments in which individual cells expressing Rab8WT–GFP were pretreated with two different siRNAs targeting each Rac1 (*n*=42 and 97) , Tiam1 (*n*=31 and 70) and Tiam2 (*n*=49 and 57), as well as with a non-targeting control (*n*=113, Ctrl). (C) HT1080 cells expressing Rab8Q67L–GFP were lysed. Pulldown assays of proteins bound to the GST-tagged PAK binding domain were immunoblotted with anti-Rac1 antibody. Representative western blot and bar diagrams illustrating densitometric analysis of the relative activities of Rac1 normalized for whole-cell lysate and expressed as a ratio to control cells are shown. Results are mean±s.e.m. (*n*=3). (D–F) Representative images obtained by confocal microscopy of immunostained HeLa cells. (D) Endogenous Tiam1 (green), Rab8 (D22D8 antibody; magenta), and Rab8 and Tiam1 overlay, where arrows indicate areas of enrichment. Tub, tubulin; Pha, phalloidin. (E) Endogenous Tiam1 (red), tubulin (purple) and phalloidin (blue), and exogenously expressed Rab8WT–GFP and Rab8Q–GFP and their overlays. (E′) Detail of area highlighted by the rectangle. (F) Endogenous Tiam1 (green or red), exogenously expressed Rab8Q67L–GFP (blue) and Hoechst 33342 (blue), as indicated. Panels show overlaid images and a segmented cell image highlighting Rab8-expressing cells (asterisks). (G–I) HeLa cells transfected with GFP, Rab8Q67–GFP or RhoV14–GFP, or Rab8Q67–GFP plus RhoV14–GFP were plated on fibronectin, fixed and stained with phalloidin, anti-vinculin antibody and Hoechst 33342. (G) Representative images showing overlaid Hoechst 33342 (blue) and GFP (green), vinculin (red), phalloidin (green) and overlaid vinculin and phalloidin staining obtained by confocal microscopy. (H,I) Box-and-whisker representations of (H) CA2 and (I) SF4 features quantified in untransfected cells (−GFP, white boxes) or cells expressing GFP, Rab8Q–GFP, or coexpressing Rab8Q67L–GFP and either GFP or RhoV14–GFP (RhoV14) and GDI (hatched boxes). Values were obtained from a representative experiment out of three independent experiments in which individual cells expressing GFP (+GFP, *n*=631) or not (−GFP, *n*=609), or expressing Rab8Q (*n*=318), Rab8Q+GFP (*n*=63), RhoV14+GDI (*n*=121), RhoV14+GDI+GFP (*n*=16) or Rab8Q+RhoV14+GDI (*n*=20) were measured. The box represents the 25–75th percentiles, and the median is indicated. The whiskers show maximum and minimum values.

To examine the effect of Rab8 on focal adhesions in migrating MDA-MB-231 cells, we expressed Rab8–GFP and paxillin tagged to orange fluorescent protein and imaged them by total internal reflection (TIRF) microscopy, revealing that Rab8 localizes at protrusive areas and at subcortical and central focal adhesion areas (Fig. 6A; Movie 1). We found significant association of Rab8-positive vesicles with focal adhesion areas (0.5 vesicles/μm^2) compared with non-focal adhesion areas (0.27 vesicles/μm^2). Live-cell TIRF imaging showed Rab8 vesicles being actively recruited to mature focal adhesions (Fig. 6B; Movies 2 and 6). Quantitative image analysis revealed a link between focal adhesion dynamics and Rab8 vesicle recruitment; vesicles associated predominantly with disassembling focal adhesions at the cell periphery, and much less with nascent focal adhesions at cortical areas (Fig. 6B,C), suggesting that Rab8 vesicle recruitment led to focal adhesion disassembly. Accordingly, volume rendering reconstruction of the dynamics of a focal adhesions marked with paxillin–mRFP revealed that continuous delivery of Rab8–GFP-positive vesicles coincides with substantial loss of focal adhesion volume (Fig. 6D; Movie 3), indicating a role for Rab8 mediating focal adhesion disassembly. We specifically addressed this issue by performing an assay to study microtubule-dependent focal adhesion disassembly (Ezratty et al., 2005). Importantly, after 1 h of nocodazole washout, control cells displayed a strong reduction in focal adhesions, whereas Rab8 KD cells displayed enlarged focal adhesions compared to control cells (Fig. 6E,F). Rab8Q67L-expressing cells had a reduced number of focal adhesions that were enlarged after nocodazole treatment and then almost completely disappeared after 30 min of nocodazole washout; in contrast, approximately 1 h was required for control cells to disassemble focal adhesions to this extent (Fig. 6E,F). Interestingly, during nocodazole treatment (focal adhesion enlargement) and washout (focal adhesion disassembly), Rab8 vesicles were enriched and had active dynamics in focal adhesion areas, indicating microtubule-independent Rab8 vesicle dynamic redistribution at focal adhesions (Fig. 6G; Movie 4).

Rab8 is critical for sustaining cell polarization and migration directionality of carcinoma cells

Our results suggest that Rab8 localization could constitute a spatio or temporal cue to perpetuate the protrusiveness of the cell surface at a specific plasma membrane location, which could promote persistency in cell migration, a matter that has not yet been established. To address this issue, we conducted a time-lapse TIRF analysis of MDA-MB-231 cells expressing Rab8wt–GFP, revealing dynamic re-localization of Rab8 to cell protrusions during directional migration (Fig. 7A; Movie 5). We explored the role of Rab8 GTPase in cell migration using MDA-MB-231 cells stably expressing shRNAs specific for Rab8. Rab8 KD cells showed an impaired chemotactic response to EGF (Fig. 7B) and wound closure (Fig. S3E,F), demonstrating that Rab8 is necessary for exogenously induced directional cell motility, in accordance with previous reports showing that the Rab8 GEF Rabin8 is a direct substrate of ERK1/2 in response to EGF signalling (Wang et al., 2015). Expression of Rab8Q67L in these cells increased their polarization, whereas Rab8 KD reduced it (Fig. 7C,D) and also impaired EGF-induced cell polarization (Fig. 7E). To study the role of Rab8 in intrinsic cell migration, we plated MDA-MB-231 cells stably expressing the Rab8 shRNAs or transiently transfected with Rab8Q67L onto fibronectin (Fn)-coated surfaces and tracked individual cell trajectories (Fig. 7F). The cell trajectories were used to measure the directionality index and the migration velocity (Fig. 7G,H). Rab8 KD and, to a lesser extent, expression of Rab8Q67L, impaired persistent migration, although velocity was not significantly affected by Rab8 expression or activation (Fig. 7F–H). Like Rab8Q67L expression, restoration of Rab8 in KD cells by expression of the shRNA-insensitive mutant (Rab8^{mut}) did not affect migration speed but had a mild negative effect on migratory persistency (Fig. 7G,H). Taken together, these results reveal that Rab8 mediates directional migration by regulating the homeostasis of Rho GTPases (Rac1 and RhoA), thereby reorganizing the actin cytoskeleton and focal adhesions. Our results additionally define a mechanism of Rab8-regulated focal adhesion disassembly mediated by the proteases calpain and MT1-MMP independently of Rho GTPases (Fig. 8).

DISCUSSION

In the present study, we have established an HCA tool that extracts quantitative measurements of actin and focal adhesion organization with subcellular resolution, which was used to study molecular pathways regulating Rab8-mediated cytoskeletal organization. This tool assigns extracted parameters to cytoskeletal rearrangement signatures elicited by the expression of a GFP-tagged construct, and these signatures can be challenged by external perturbation such as siRNA knockdown or specific drug inhibition. We demonstrate that a fine regulation of Rab8 localization at the plasma membrane

Journal of Cell Science (2016) 129, 1734-1749 doi:10.1242/jcs.174920

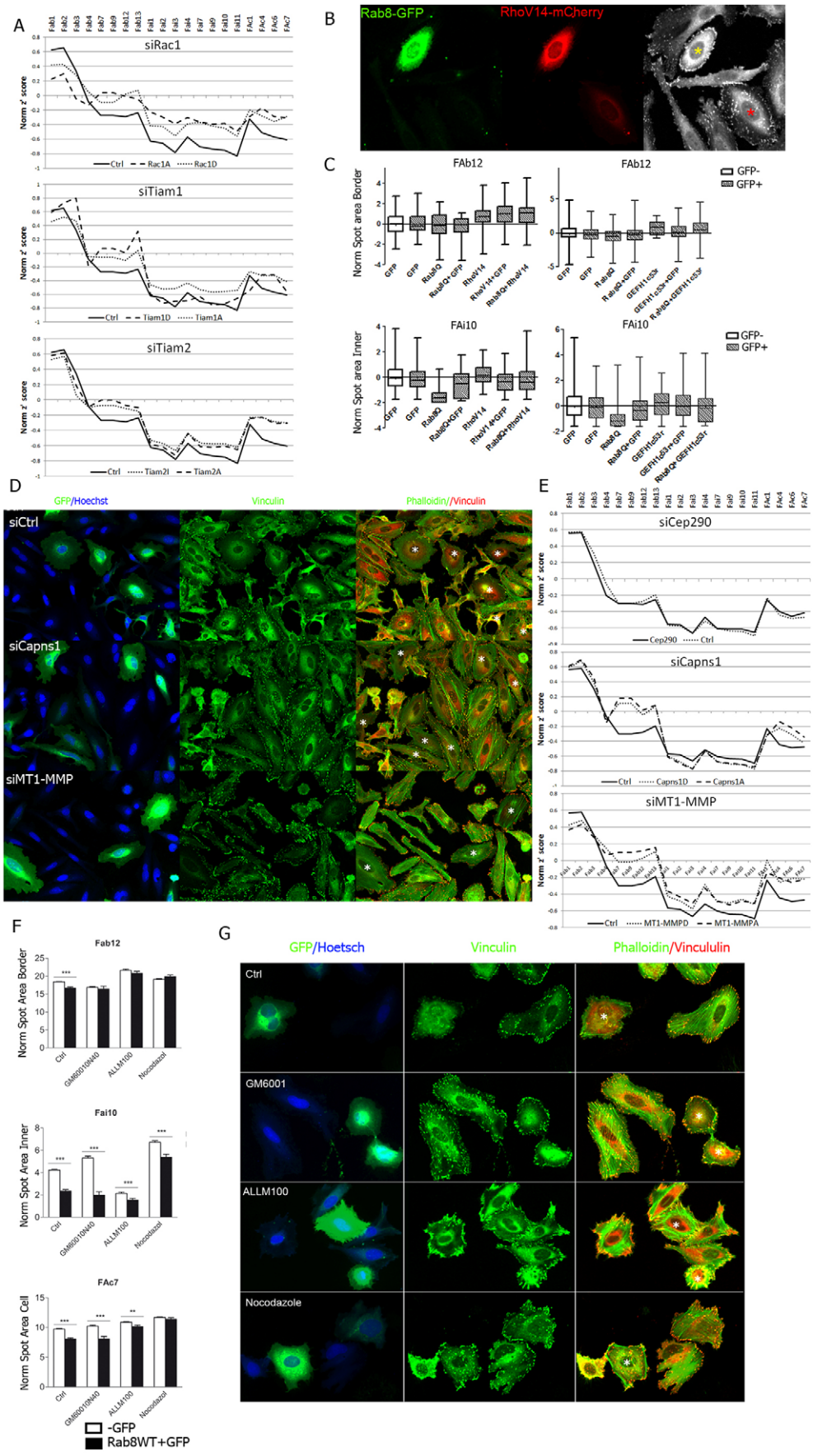

Fig. 4. See next page for legend.

Journal of Cell Science

Journal of Cell Science (2016) 129, 1734-1749 doi:10.1242/jcs.174920

Fig. 4. Rab8-promoted focal adhesion loss is microtubule-, MT1-MMP- and calpain-dependent. (A) HeLa cells were pretreated with two different siRNAs targeting the indicated genes, then transfected with Rab8WT–GFP and stained with phalloidin, anti-vinculin antibody and Hoechst 33342. Phenotypic profiles of focal adhesion rearrangements were obtained as detailed in Fig. 3B. (B) HeLa cells were transfected with Rab8WT–GFP (green) and RhoV14–mCherry (red) and stained with anti-vinculin antibody, shown in the black-and-white image, in which a double-positive cell is marked with a yellow asterisk and single RhoV14–mCherry expressing cell is marked with a red asterisk. (C) HeLa cells were transfected with GFP or Rab8WT–GFP and either RhoV14–GFP or GEFH1c53r–GFP, then stained with phalloidin and anti-vinculin antibody and analysed by HCA. Graphic representations are shown of border focal adhesions (Fab12) and inner focal adhesions (Fai10) in GFP-positive (grey boxes) and -negative cells (white boxes). For the GEFH1 experiment (left panel) individual cells expressing GFP (+GFP, *n*=298) or not (–GFP, *n*=783), or expressing Rab8Q (*n*=176), Rab8Q+GFP (*n*=90), GEFH1c53r (*n*=30), GEFH1c53r+GFP (*n*=298) or Rab8Q+GEFH1c53r (*n*=90) were measured. For the RhoV14 experiment (right panel) cells were analysed as indicated in Fig. 3H. The box represents the 25–75th percentiles, and the median is indicated. The whiskers show the maximum and minimum values. (D–G) HeLa cells were pretreated with (D,E) siRNAs targeting the indicated genes, (F,G) chemical inhibitors of MMPs (GM110) or calpain (ALLM100), or a microtubule-disrupting agent (nocodazole), and then transfected with Rab8WT–GFP and stained with phalloidin, anti-vinculin antibody and Hoechst 33342. (D,G) Representative images of cells treated as indicated. Images show overlay views of Rab8WT–GFP and Hoechst 33342 staining (green and blue) revealing nuclei and Rab8-expressing cells, vinculin immunostaining (green), and vinculin and phalloidin overlay (green and red) showing focal adhesions and polymerized actin. Rab8-expressing cells are marked with asterisks. (E) Phenotypic profiles of focal adhesion rearrangements for the siRNA treatments indicated. Values represent mean *Z*-scores obtained from one representative experiment out of three independent experiments in which individual cells expressing Rab8WT–GFP were pretreated with the siRNAs indicated. siCep290 (*n*=416), two different siCapns1 oligonucleotides (*n*=173 and 66), two different siMT1-MMP oligonucleotides (*n*=60 and 124) and siCtrl (*n*=585). (F) Quantification of focal adhesion area analysed in the cell border (Fab12), inner (Fai10) and whole cell (FAc7) regions of untransfected (−GFP) and RabWT-GFP expressing (Rab8WT+GFP) HeLa cells pretreated with the indicated inhibitors. Values are obtained from one representative experiment out of three independent ones in which individual cells expressing Rab8WT–GFP or not (−GFP; *n*=1264, 185, 186 and 545, and Rab8WT+GFP; *n*=219, 32, 84 and 136 for GM600, ALLM, and Nocodazole pretreatments, respectively). (between the experimental and control values as evaluated by a two-tailed Mann–Whitney test).

accompanies cell protrusive activity, and that Rab8 is crucial for determining the directionality of cell locomotion, given that both its widespread activation and knockdown negatively impacted upon persistent migration. Although previous reports have established that Rab8 promotes actin rearrangements (Hattula et al., 2006; Peränen et al., 1996), the underlying mechanism had not been explored in depth. Our findings demonstrate that expression of constitutively active Rab8 induces an increase in cortical actin that was impaired by knocking down either Rac1 or its GEF Tiam1, indicating that Rac1 activity is responsible for Rab8-mediated cortical actin polymerization. In addition, Tiam1 and Rac1 colocalized at plasma membrane protrusions, and Rab8 activation led to the mobilization of Tiam1 from intracellular storage compartments in confluent monolayers and to the activation of Rac1. We therefore propose a model in which Rab8 promotes redistribution of Tiam1 to the plasma membrane, where it activates Rac1 to promote cortical actin polymerization, leading to protrusive activity. This is consistent with earlier studies showing that Rac1 undergoes Tiam1-dependent activation in Rab5-containing endosomes and during Arf6-mediated recycling to the plasma membrane, leading to actin polymerization in dorsal ruffles (Palamidessi et al., 2008). Although Arf6 and Rab8 have been shown to colocalize in tubular structures (Hattula et al., 2006), we did not observe colocalization of Rab8 and Tiam1 in tubules, but mainly at protrusion sites in the plasma membrane, suggesting that Rab8 acts downstream of Arf6 to promote Rac1 activation by mediating docking and fusion of Tiam1-carrying recycling endosomes. Interestingly, Rab8 promotes the delivery of cholesterol to the plasma membrane (Kanerva et al., 2013), which would provide cholesterol-rich membrane microdomains where Rac1 can activate its downstream effectors (Navarro-Lérida et al., 2012). In addition, Rab8 promotes Rac1-independent and RhoA-dependent disassembly of stress fibre. Given that Rac1 and RhoA are mutually antagonistic, Rab8-mediated loss of stress fibre could be an indirect effect of activated Rac1-mediated RhoA inhibition. However, this is not the case, as Rac1 knockdown was unable to compensate for Rab8-induced stress fibre disassembly, showing that other pathways are involved. Recent work has found that DLC3 (also known as STARD8), a Rho-specific GTPase-activating protein (GAP) that is associated to Rab8 tubules regulating RhoA activity in the recycling compartment (Braun et al., 2015), could be mediating this effect. We tested candidate genes related to Rab8 function (Ocrl, Cep290) and kinases with homology to known Rab8 effectors (TNIK, MINK and HGK), using a high-content imaging approach; however, none of them yielded positive results.

Interestingly, our study revealed that Rab8-positive vesicles are associated with focal adhesions, promoting their disassembly, which suggests the involvement of the so-called ‘relaxing factor’ transported through the microtubule network to focal adhesions to mediate their disassembly (Kaverina et al., 1999; Small and Kaverina, 2003). Although the involvement of RhoA in Rab8-mediated focal adhesion loss could not be discarded, our studies reveal the existence of additional Rho-independent mechanisms. Calpain and MT1-MMP proteases were both involved in Rab8-mediated disassembly. Rab8 KD impairs vesicular localization of both Calpain and MT1-MMP proteases, an evidence for Rab8-mediated trafficking of these proteases, although lack of colocalization with Calpain suggest they converge at plasma membrane from independent trafficking pathways. Previous work has revealed that Rab8 co-distributes with MT1-MMP during vesicle transport to the plasma membrane, promoting cell invasion (Bravo-cordero et al., 2007). Inhibition of MMPs increased the central distribution of focal adhesions, whereas the calpain protease inhibitor led to a cortical distribution of these structures. These differences suggest that each type of protease plays a distinct role in focal adhesion organization, with MT1-MMP probably affecting sliding and/or central and rear focal adhesion disassembly. This could explain why even though both proteases are involved in Rab8-dependent focal adhesion disassembly, neither is sufficient on its own to completely abolish disassembly mediated by Rab8.

Although nocodazole completely abolished Rab8-mediated disassembly of focal adhesions, demonstrating its microtubule dependence, dynamic recruitment of Rab8 vesicles to focal adhesions remained unaffected during nocodazole treatment, revealing that subcortical trafficking of Rab8-positive vesicles is microtubule independent. Rab8-positive vesicles could be dynamically recruited to the plasma membrane by cortical actin-mediated transport through interaction with its effectors MyoVa and MyoVb, actin-based motors (Khandelwal et al., 2013; Roland et al., 2007). Rab8 likely allows delivery of microtubule-dependent vesicular cargo to the plasma membrane, acting on the switch between microtubule and actin filament networks through its effector MyoVa, as reported for Rab8-mediated GLUT4 exocytic trafficking in response to insulin (Sun et al., 2014). Microtubule network depolymerization with nocodazole, could thus be trapping Rab8 vesicles in a futile cycle along the meshwork of cortical actin,

Journal of Cell Science (2016) 129, 1734-1749 doi:10.1242/jcs.174920

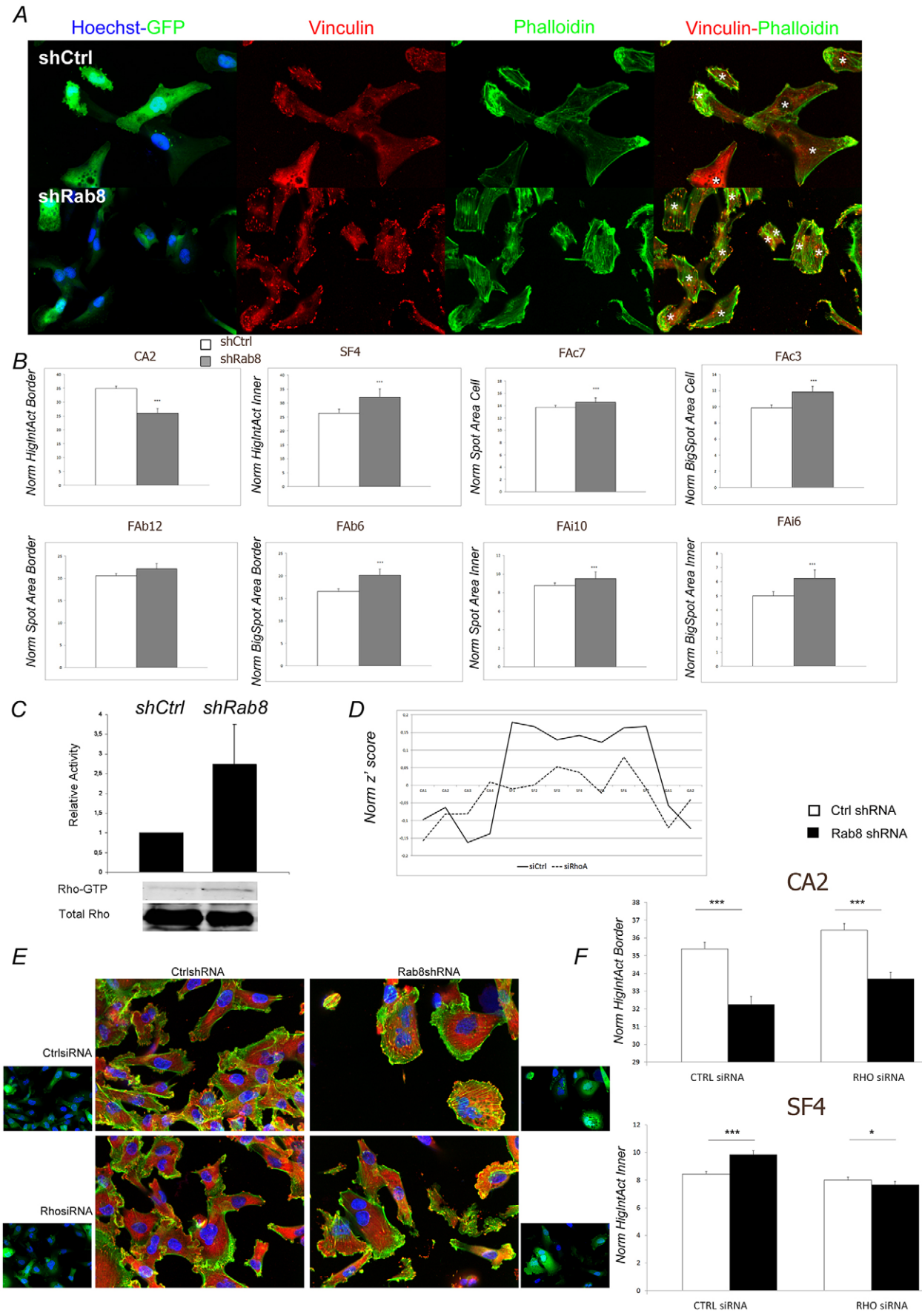

Fig. 5. See next page for legend.

Journal of Cell Science (2016) 129, 1734-1749 doi:10.1242/jcs.174920

Fig. 5. Rab8 knockdown promotes RhoA-dependent loss of stress fibres in carcinoma cells. (A,B) MDA-MB-231 cells stably expressing control shRNA (shCtrl) or Rab8 shRNA-1 (shRab8) tagged with GFP were plated on fibronectin, then fixed and stained with phalloidin or anti-vinculin antibody to reveal actin and focal adhesions. (A) Representative fluorescence confocal images show GFP (green) Hoechst 33342 (blue), vinculin (red) and phalloidin (green) stains and their overlay as indicated. Asterisks depict GFP-positive cells expressing the indicated constructs. (B) Quantification of cortical actin, stress-fibre- and focal-adhesion-related features by HCA from GFP-positive cells expressing Ctrl (n=93) and Rab8 (n=23) shRNAs. (C) Relative RhoA activity in MDA-MB-231 cells expressing either non-targeting shRNA (shCtrl) or Rab8 shRNA-1 (shRab8). Pulldown assays of proteins bound to GST-tagged rhotekin-binding domain were immunoblotted with anti-RhoA antibody. The graph illustrates densitometric analysis of relative RhoA activity, normalized to values in whole-cell lysates and expressed as a ratio to the value in control cells. (D–F) MDA-MB-231 GFP-positive cells stably expressing control shRNA (shCtrl) or Rab8shRNA-1 (shRab8) were treated with non-targeting siRNA (siCtrl) or RhoA-targeting siRNA (siRhoA), and then stained with phalloidin and anti-vinculin antibody to reveal actin and focal adhesions. (D) Actin rearrangement profile obtained by HCA from GFP-expressing Rab8 shRNA (shRab8) for the siRNA treatments indicated. Values represent mean Z-scores obtained from one representative experiment out of three independent experiments in which individual cells expressing shRab8 were pretreated with Ctrl (n=474) or RhoA (n=593) siRNAs. (E) Representative fluorescence confocal images showing overlay of phalloidin (green), Hoechst 33342 (blue), and vinculin (red) or Hoechst 33342 and GFP (thumbnails). (F) Graphic representations of mean±s.e.m. values of cortical actin (CA2) and stress fibre (SF5) features obtained from cells expressing either shCtrl and pretreated with siCtrl (n=825) or siRho (n=476), or siRhoA-expressing cells pretreated with siCtrl (n=735), or siRhoA (n=595). (B,D,F) Values represent mean±s.e.m. and were obtained from one representative experiment out of three independent experiments. *P<0.05; ***P<0.001 (between the experimental and control values as evaluated by a two-tailed Mann–Whitney test).

which would require microtubule-mediated delivery of either a GEF or an effector protein for Rab8 to allow focal adhesion disassembly.

Recent work has established that CLASP proteins mediate microtubule tethering at focal adhesions, leading to the delivery of Rab6-positive exocytic vesicles to regulate adhesion turnover (Stehbens et al., 2014). Accordingly, Rab8 has been shown to be involved in secretory trafficking, being recruited to vesicles by interacting with Rab6 and mediating the docking and fusion of exocytic carriers to the plasma membrane in a manner dependent on its interaction with the MICAL3–ELKS complex, which binds to LL5β (also known as PHLDB2) located at the plasma membrane (Grigoriev et al., 2011). In fact, LL5β is enriched at focal adhesions and at the leading edge of migrating cells, and thus could represent the local cue leading to Rab8 localization at these sites (Lansbergen et al., 2006; Stehbens et al., 2014). The study of Rab8 activation at the subcellular level should prove to be very useful for understanding its mechanism of action. In this regard, our studies show that overexpression of the wild-type form of Rab8 induces formation of multiple prominent protrusions, whereas the constitutively active mutant induced a generalized protrusive effect on the whole cell perimeter, suggesting that local activation of Rab8 at the plasma membrane is crucial to ensuring persistent and locally constrained protrusion. A good candidate mediator of the Rab8-activating process is the Rab8 GEF Rabin8, a Rab11 effector enriched in membrane protrusions (Hattula et al., 2002) and responsible for Rab8-mediated apical exocytosis during lumen formation (Bryant et al., 2010). Alternatively, because the Sec15p subunit of the exocyst is an effector of the yeast Rab8 homolog (Guo et al., 1999), the exocyst might well provide a local cue to promote vesicle tethering by interacting with Rab8-decorated vesicles. Accordingly, it has been implicated in directional cell migration, actin polymerization and delivery of MT1-MMP to the plasma membrane (Letinic et al., 2009; Liu et al., 2009; Monteiro et al., 2013; Sakurai-Yageta et al., 2008; Spiczka and Yeaman, 2008). Taken together, our results support the hypothesis that Rab8 acts as a plasma membrane hub converging secretory and recycling trafficking routes through Rab6-, and Rab11- and Rabin8-dependent mechanisms, respectively.

Our work offers a new perspective on how membrane trafficking and cytoskeletal rearrangements are integrated, with Rab8-mediated trafficking constituting a nexus that integrates vesicular transport with signalling modules for actin polymerization and focal adhesion turnover to stimulate cell polarization and persistent migration. Given the recent reports demonstrating involvement of Rab8 in stretch-regulated exocytosis (Khandelwal et al., 2013), it is possible that mechanosensory elements provide the local stimulatory signal triggering Rab8 activity. In this regard, the HCA results presented here show that silencing TRPM7, a stretch-activated cation channel, affects the Rab8-induced cytoskeletal rearrangement profile, a matter that deserves further study. Rab8 could respond to local tension by regulating the recruitment of recycling and/or secretory vesicles to plasma membrane locations where it would deliver cargo of regulatory or structural components to perpetuate the protrusive activity, thus promoting directional movement.

MATERIALS AND METHODS

Cell culture, transfection and stable cell line generation

Human MDA-MB-231, HeLa and HT1080 cells were from the ATCC (Manassas, VA, USA) and were maintained in Dulbecco's modified Eagle's medium (DMEM) supplemented with 10% fetal bovine serum (FBS) and F12K medium, respectively. Mycoplasma tests were performed every two months. The Rab8Q67L–GFP, Rab8WT–GFP, Rab8^{mut}–mRFP and constitutively active GEF-H1^{c53r} constructs were as described previously (Bravo-cordero et al., 2007; Pathak et al., 2013). The Rab8 rescue construct (Rab8^{mut}) carries four silent mutations in the Rab8 shRNA target sequence. RhoV14–GFP and paxillin–GFP were as described previously (Grande-García et al., 2007). Raichu FRET biosensors, Tandem FRET standard (Spectrin) were as described previously (Itoh et al., 2002; Megías et al., 2009). Cell transfection was performed using Lipofectamine 2000 (Invitrogen). Paxillin–mRFP was derived from paxillin–EGFP, kindly provided by Mark H. Ginsberg [Division of Rheumatology, Allergy & Immunology, University of California, San Diego (UCSD), CA] (Grande-García et al., 2007).

Chemical inhibitors, antibodies and staining reagents

The microtubule-disrupting agent nocodazole was from Sigma, the MMP inhibitor GM6001 from Millipore, and the calpain inhibitor ALLM from Calbiochem. Monoclonal antibodies were commercially validated and were used and obtained as follows: anti-Rac1 (T-17) polyclonal antibody (2 µg/ml), anti-RhoA (26C4) (2 µg/ml) and anti-Tiam1 (F-11) (4 µg/ml; Santa Cruz Biotechnology), anti-Rab8 (4/Rab4) (2 µg/ml; BD Biosciences) and D22D8 (1/100; Cell Signaling), anti-vinculin (V9131) (2 µg/ml) and anti-talin (8D4) (Sigma-Aldrich), and anti-Capns1 (3C4) (1 µg/ml) (antibodies-online.com) antibodies. Anti-MT1-MMP Lem 2/15 was previously validated and used at 20 µg/ml (Gálvez et al., 2001). Alexa-Fluor-546-, -594-, -680- or 647-conjugated anti-mouse-IgG monoclonal antibodies, phalloidin, Cell Mask Blue and Hoechst 33342 or DAPI (4′,6-diamidine-2-fenilindol) for staining actin, cytoplasm and nuclei, respectively, were all purchased from Invitrogen.

Protein knock down by shRNA and siRNA

MDA-MB-231 cells stably expressing Rab8A shRNA 1/2 have been described elsewhere (Bravo-cordero et al., 2007). Western blotting was used to confirm stable knockdown of Rab8 (Fig. S2B). siRNAs from ON-

Journal of Cell Science (2016) 129, 1734-1749 doi:10.1242/jcs.174920

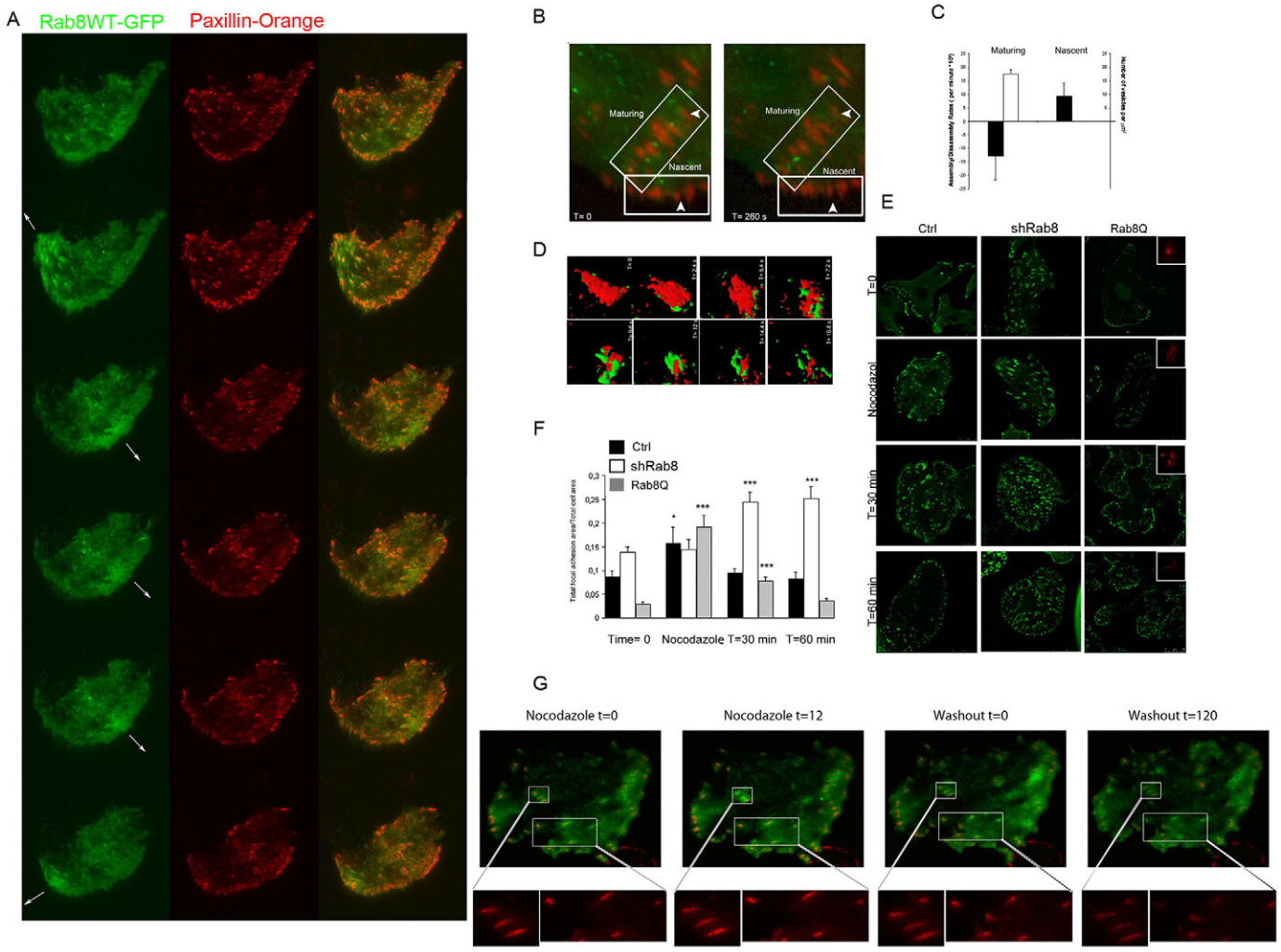

Fig. 6. Rab8 localizes to focal adhesions and induces their disassembly during carcinoma cell migration. (A,B) Live-cell TIRF imaging of MDA-MB-231 cells transfected with Rab8WT–GFP and paxillin–mRFP. (A) Representative images showing the association of Rab8-positive vesicles to focal adhesions during cell protrusion, from Movie 1. Arrows indicate the direction of cellular protrusions. (B) Images, obtained at the indicated time points from Movies 2 and 6, depicting an area in which mature focal adhesion disassembly occurs and the area of nascent focal adhesions. Arrowheads point to focal adhesions. (C) Average rate constants for focal adhesion assembly and disassembly measured for ten focal adhesions in zones 1 and 2 from the time-lapse experiment corresponding to Movie 6 (open bars). The number of vesicles delivered to these areas per μm^2 is also shown (filled bars); n=10. (D) Surface-rendered reconstruction of focal adhesion disassembly obtained from a time-lapse TIRF experiment (Movie 3). (E,F) MDA-MB-231 cells stably expressing non-targeting shRNA (Ctrl) or Rab8 shRNA-1 (shRab8), or transiently expressing Rab8Q67L–GFP, were plated on fibronectin and treated with 10 µM nocodazole (Noco), focal adhesion organization was assessed by vinculin immunostaining. Values represent mean±s.e.m. values from individual Ctrl cells (n=26, 10, 12 and 8 for t=0, Noco, t=30 and t=60, respectively), shRab8-expressing cells (n=17, 6, 7 and 12 for cells at t=0, Noco, t=30 and t=60, respectively), and Rab8Q-expressing cells (n=13, 4, 7 and 4 for cells at t=0, Noco, t=30 and t=60, respectively) obtained from one representative experiment out of three independent ones. (E) Confocal images showing vinculin immunostaining (green) and expression of Rab8Q67L–GFP (red cells in insets) were obtained before (t=0) or after 4 h of nocodazole treatment (Nocodazole), as well as 30 or 60 min after nocodazole washout (t=30 and t=60, respectively). (F) Relative focal adhesion area calculated for whole cells (FAc7) expressing the different constructs and undergoing the indicated treatments. (G) Representative TIRF images from MDA-MB-231 cells transfected with Rab8WT–GFP and Paxillin–mRFP during nocodazole treatment (t=0 and 12) and after washout (t=0 and 120) from Movie 4. Upper images show overlaid Rab8 and paxillin signals, whereas lower images show the paxillin signal from highlighted focal adhesion areas for the times and treatments indicated. Values represent mean±s.e.m. *P<0.05; ***P<0.001 (between the experimental and control values as evaluated by Student's t-test).

TARGETplus (Thermo Fisher Scientific Inc.), Silencer select (Ambion, Life Technologies, Carlsbad, CA, USA), and Stealth (Invitrogen) collections were used for silencing the different genes. Sequences are specified in Table S2. HeLa and MDA-MB-231 transfection with siRNAs was performed using the solid-phase reverse transfection protocol (Erfle et al., 2008). Plates were prepared automatically using the Freedom Evo 2000 robot (TECAN, Männedorf, Switzerland), and dried on a Speed Vac. Cells were seeded on top of dried assay plates, and wells were either processed for quantitative real-time RT-PCR (qRT-PCR) after 24 h for assessment of mRNA knockdown (Fig. S4A,B) or subjected to phenotypic HCA as specified.

Phenotypic HCA for cellular CSK rearrangements

Cells were seeded on top of siRNA pre-coated plates, then transfected with GFP or GFP fusions (Rab8WT or Rab8Q). Cells were fixed, permeabilized, and stained with anti-vinculin Alexa-Fluor-546-conjugated and anti-mouse-IgG secondary antibody, Alexa-Fluor-647–phalloidin, Cell Mask Blue and Hoechst 33342. Images were acquired with an Opera confocal microscope (Perkin Elmer, Waltham, MA) and analysed with a code developed using Definiens developer software version XD2 (Definiens AG, Germany), which can be obtained upon request. A detailed description of the image analysis procedure is described in Fig. S1. An established data-mining pipeline based on cell biology metrics described previously (Azegrouz et al.,

Journal of Cell Science (2016) 129, 1734-1749 doi:10.1242/jcs.174920

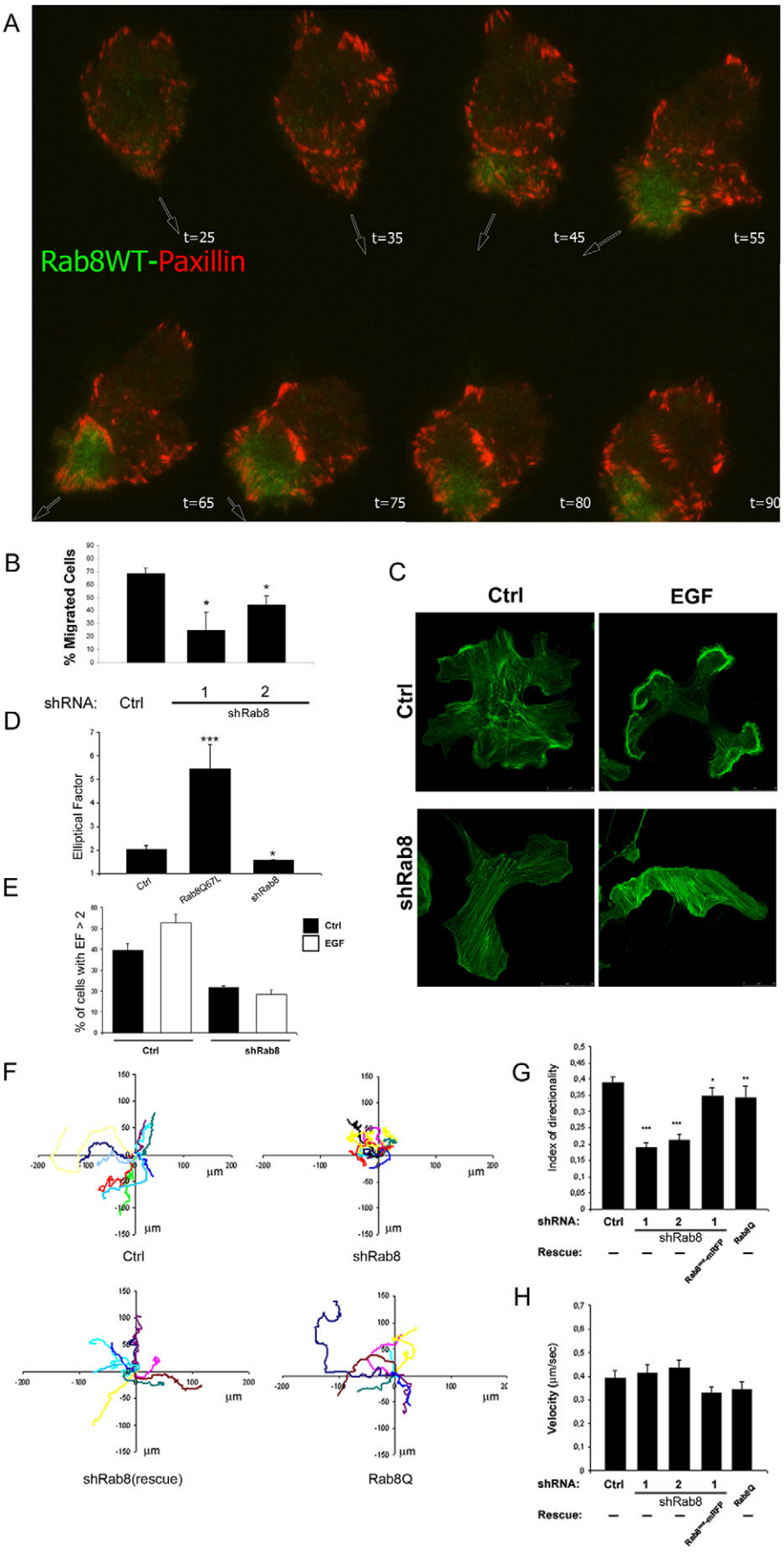

Fig. 7. Rab8 regulates cell migration.
(A) Representative live-cell TIRF images of MDA-MB-231 cells transfected with Rab8WT–GFP and Paxillin–mRFP. Arrows indicate direction of movement (Movie 5). (B–H) MDA-MB-231 cells were transfected to stably express control shRNA (Ctrl), Rab8 shRNA-1 and -2 (shRab8), Rab8 shRNA-1 plus Rab8^{mut} (Rescue, carrying mutations in the Rab8 shRNA target sequence), or to transiently express Rab8Q67L–GFP. (B) Cells were allowed to migrate for 48 h on transwell filters coated with fibronectin towards an EGF gradient. Bars represent the percentage of migrated GFP-expressing cells quantified in four different fields of one filter from three independent experiments. (C–E) Cells were stained with phalloidin and imaged by confocal microscopy. (C) Representative images. (D) Elliptical Factor averaged from Ctrl (*n*=31), and cells expressing Rab8Q67L (*n*=11) and shRab8 (*n*=18) from two independent experiments. (E) Percentage of cells with elliptical factor >2 obtained from cells expressing shCtrl (*n*=19 and 31 for EGF-treated and untreated, respectively), or shRab8 (*n*=18 and 16 for EGF-treated and untreated, respectively) from two independent experiments. Values represent mean±s.e.m. (F–H) Cells were plated on 20 µg/ml fibronectin and recorded in random migration by time-lapse microscopy over 16 h (10-min frame interval). (F) Plots show representative migration tracks of the cells expressing the constructs indicated below each graph. (G,H) Directionality index and mean velocities measured for expressing each construct. Values represent mean±s.e.m. obtained from individual cells expressing shCtrl (*n*=89), shRab8_1 (*n*=87), shRab8–2 (*n*=62), shRab8+Rab8mut (*n*=41) and Rab8Q (*n*=31) from two independent experiments. **P*<0.05; ***P*<0.01; ****P*<0.001 (between the experimental and control values as evaluated by Student's *t*-test).

Journal of Cell Science

Journal of Cell Science (2016) 129, 1734-1749 doi:10.1242/jcs.174920

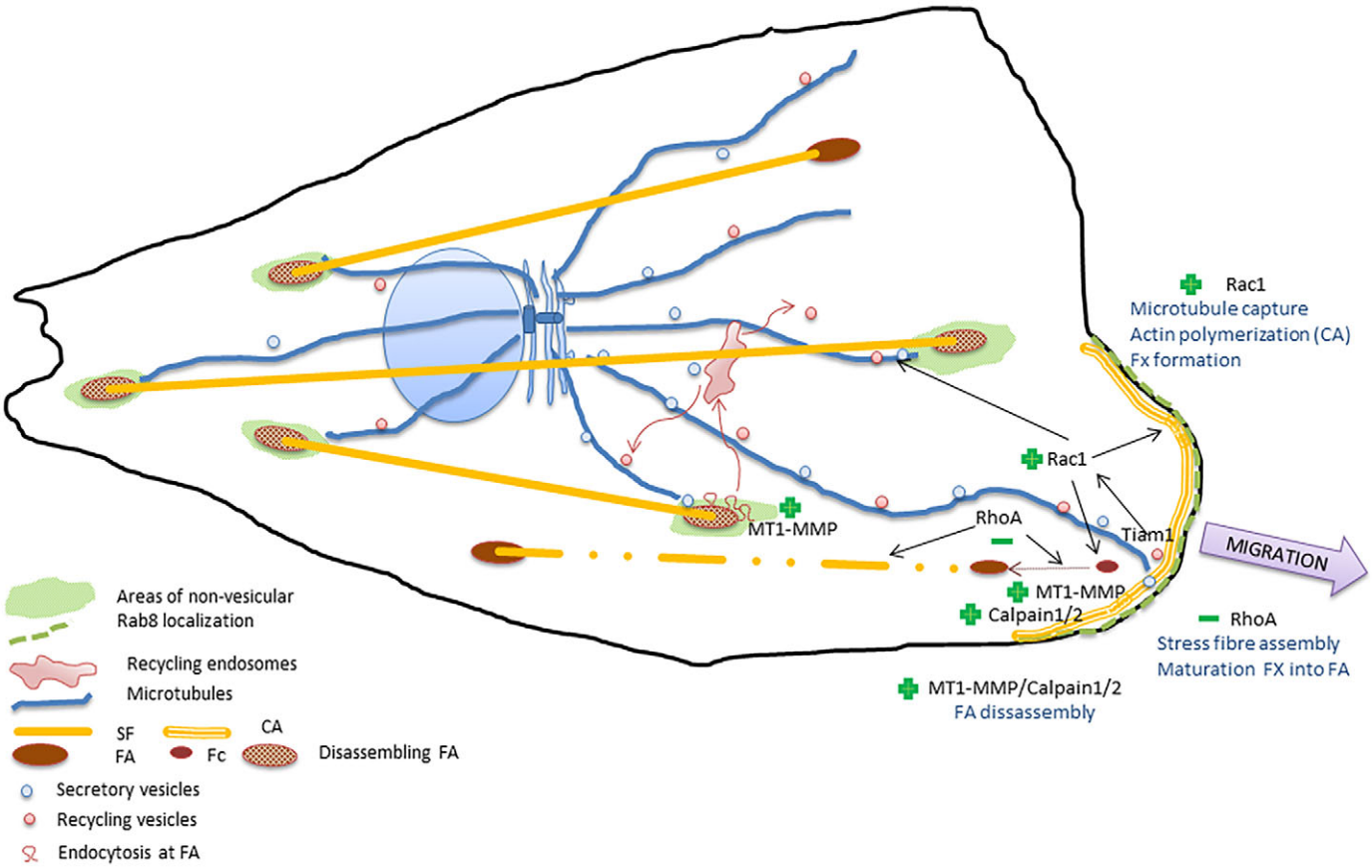

Fig. 8. Model of Rab8-mediated cytoskeletal rearrangements during cell migration. The figure depicts a migrating cell, with a protrusion area schematized at the bottom right, where Rab8 localizes at the plasma membrane and Rac1 becomes activated through Tiam1 delivery, leading to cortical actin polymerization, formation of nascent focal adhesions (Fc) and the capture of microtubules to generate mature focal adhesions. Low RhoA activity prevents focal adhesion maturation and assembly of stress fibres (SF). The proteases MT1-MMP and calpain are also recruited, leading to focal adhesion turnover at these sites. Rab8 also localizes at inner focal adhesion sites, where trafficking of MT1-MMP leads to their disassembly. CA, cortical actin; FA, focal adhesion.

2013) was used as a quality control to discard outlaying cells such as: poor or excessively spread, highly confluent or poorly stained cells, among others (Fig. S1). Normalized *Z*-scores were computed for each feature by subtracting the mean of controls (untransfected cells) from the computed value for cells expressing GFP-tagged constructs (GFP, Rab8–GFP or Rab8Q–GFP) and dividing the result by the s.d. of the controls (untransfected cells) as described previously (Collinet et al., 2010). In the case of Rab8 KD experiments, normalization was performed with non-targeting control (shCtrl) construct. Assessment of siRNA transfection efficiency was carried out in INCENP-siRNA-containing wells to calculate the Z' factor for every assay plate based on the difference of INCENP siRNA to control non targeting siRNA (Fig. S4C,D). Plates were further processed for HCA of cytoskeletal phenotypes only when Z' factor values computed were above 0.35. Mean Z' values obtained for the different plates analysed was 0.70 with a s.e.m. of 0.04.

Immunofluorescence staining and imaging

Immunofluorescence staining was performed in cells attached to glass coverslips pre-coated with 20 µg/ml fibronectin (Fn) for 4 h. Cells were fixed at 4°C for 5 min with 4% paraformaldehyde and permeabilized with 0.5% Triton X-100 and stained with the appropriate antibodies. TIRF imaging was performed with a Leica TIRF microscope fitted with a HCX Pl APO 100×1.46 NA oil objective. Confocal imaging was carried out with a Leica TSC SP5-RS AOBS fitted with a HCX Pl APO 63×1.32 NA oil objective (Leica Mannheim. Germany). Bright-field images for wound-healing assays were acquired using a Leica DMI6000 fitted with a HCPL Fluotar 5×0.15 NA objective. High content imaging of cytoskeletal rearrangements was performed with an Opera automated confocal microscope (Perkin Elmer, Waltham, MA) fitted with an NA=0.7 water immersion objective at a magnification of 20×. Images shown in figures were typically processed using levels or contrast tools using Adobe Photoshop (Adobe SI, San Jose, CA, USA) enhancing image contrast of the different fluorescence signals in entire images.

Cell migration and polarization experiments

Chemotaxis assays were performed in 8-mm-pore Transwell chambers from Costar (Corning) coated with 20 µg/ml fibronectin. Cells were resuspended in serum-free medium, seeded at 5×10^4 cells/well, and allowed to transmigrate towards 10 µM EGF medium for 48 h, and then counted at the top and bottom of the chamber using Imaris software (Bitplane AG, Zurich, Switzerland). Graphs represent the percentage of GFP- expressing, or mRFP- or GFP-expressing (for the rescue) migrated cells. Cells expressing different constructs and treated or not with EGF were imaged by confocal microscoy. Elliptical factor was calculated using Metamorph software (Universal Imaging) based on a thresholding quantification of fluorescence images immunostained with phalloidin. Random cell migration experiments were imaged using a Leica DMI6000 with a 20× HC-Plan APO 0.7 NA objective.

Focal adhesion dynamic studies

Cells expressing paxillin–mRFP were imaged using a Leica TIRF microscope. Quantification of the number of vesicles within focal adhesions versus non-focal-adhesion areas was carried out by drawing circular regions overlaid on each cellular focal adhesion (focal adhesion area). Equal numbers of circular regions were drawn in areas where no focal adhesions were found (non-focal-adhesion area), which were superimposed

on the corresponding Rab8WT–GFP image and the number of vesicles per region was counted. The ratio of the total focal adhesion area to the total cell area was calculated for each cell using Metamorph software (Universal Imaging), based on a thresholding quantification of immunofluorescence-stained paxillin. Focal adhesion dynamics were quantified for the image series of MDA-MB-231 cells expressing paxillin–mRFP. The assembly to disassembly ratio equals the [assembly/disassembly ratio=($Area_f$−$Area_i$)/total time (min)], with $Area_f$ being the final area and $Area_i$ the initial area of each focal adhesion. The number of vesicles per adhesion was scored by measuring the number of Rab8 vesicles per μm^2 of focal adhesion in the whole experiment.

Pulldown assays and western blot analysis

MDA-MB-231 control cells or those knocked down for Rab8 (shRNA1), or HT1080 cells expressing GFP or Rab8Q67L, were plated on 20 µg/ml fibronectin and serum starved for 1 h, then stimulated with 10 µM EGF for 30 min. Rac1 and RhoA activities were determined by pull-down assay as described (Grande-García et al., 2007).

Acknowledgements

We thank Ira Mellman, Mark H. Ginsberg, Celine DerMardirossian, Michiyuki Matsuda and Roger Y. Tsien for providing us with constructs. Ignacio Cotillo, Irene Palacios, Mariano Vitón and Raquel Nieto for excellent technical assistance. Gopal Karemore, Daniel Jimenez Carretero and Laura Fernandez for support with data analysis, and J. Zimmermann and A. Kirsch for assistance in software development. The CNIC is supported by the Spanish Ministry of Economy and Competitiveness (MINECO) and the Pro CNIC Foundation, and is a Severo Ochoa Center of Excellence (MINECO award SEV-2015-0505).

Competing interests

The authors declare no competing or financial interests.

Author contributions

J.J.B.-C. established stable Rab8 shRNA cell lines, contributed to the initial study design, designed and performed cell migration and focal adhesion dynamic analysis, and helped write the manuscript. M.C. established and characterized stable Rab8 shRNA cell lines, and performed HCA characterization of these cells. S.F.S. performed talin blot analysis and immunofluorescence studies. B.D., C.M.-A. and M.C.-A. conducted immunofluorescence, TIRF imaging and HCA. M.C.G. performed Rho GTPase pulldown assays. C.B., I.E. and D.G.-P. contributed to the initial design of high content analytical tools. M.A.d.P. provided funding, resources, discussed results, gave conceptual advice and contributed to manuscript writing. M. C.M. designed the study, supervised the project, developed the Definiens ruleset for HCA, analyzed HCA data, prepared figures and wrote the manuscript.

Funding

This work was supported by a grant from the Instituto de Salud Carlos III (ISCIII) [grant number FIS PI09/1028 to M.C.M.]; and Ministerio de Economía Y Competitividad (MINECO) [grant number BIO2014-62200-EXP to M.C.M, and SAF2008-02100, SAF2011-25047 and CONSOLIDER CSD2009-00016 to M.A.d.P.]. J.J.B.-C., B.D. and C.M.-A. were funded by fellowships from the MINECO, and M.C.-A. by the FIS.

Supplementary information

Supplementary information available online at
http://jcs.biologists.org/lookup/suppl/doi:10.1242/jcs.174920/-/DC1

References

Ang, A. L., Fölsch, H., Koivisto, U.-M., Pypaert, M. and Mellman, I. (2003). The Rab8 GTPase selectively regulates AP-1B–dependent basolateral transport in polarized Madin-Darby canine kidney cells. *J. Cell Biol.* **163**, 339-350.

Arjonen, A., Alanko, J., Veltel, S. and Ivaska, J. (2012). Distinct recycling of active and inactive β1 integrins. *Traffic* **13**, 610-625.

Azegrouz, H., Karemore, G., Torres, A., Alaiz, C. M., Gonzalez, A. M., Nevado, P., Salmeron, A., Pellinen, T., del Pozo, M. A., Dorronsoro, J. R. et al. (2013). Cell-Based Fuzzy Metrics Enhance High-Content Screening (HCS) Assay Robustness. *J. Biomol. Screen.* **18**, 1270-1283.

Bisi, S., Disanza, A., Malinverno, C., Frittoli, E., Palamidessi, A. and Scita, G. (2013). Membrane and actin dynamics interplay at lamellipodia leading edge. *Curr. Opin. Cell Biol.* **25**, 565-573.

Braun, A. C., Hendrick, J., Eisler, S. A., Schmid, S., Hausser, A. and Olayioye, M. A. (2015). The Rho-specific GAP protein DLC3 coordinates endocytic membrane trafficking. *J. Cell Sci.* **128**, 1386-1399.

Bravo-cordero, J. J., Marrero-Diaz, R., Megías, D., Genís, L., García, M. A., Arroyo, A. G. and Montoya, M. C. (2007). MT1-MMP proinvasive activity is regulated by a novel Rab8-dependent exocytic pathway. *EMBO J.* **26**, 1499-1510.

Bryant, D. M., Datta, A., Rodríguez-Fraticelli, A. E., Peränen, J., Martín-Belmonte, F. and Mostov, K. E. (2010). A molecular network for de novo generation of the apical surface and lumen. *Nat. Cell Biol.* **12**, 1035-1045.

Caswell, P. T., Chan, M., Lindsay, A. J., McCaffrey, M. W., Boettiger, D. and Norman, J. C. (2008). Rab-coupling protein coordinates recycling of alpha5beta1 integrin and EGFR1 to promote cell migration in 3D microenvironments. *J. Cell Biol.* **183**, 143-155.

Collinet, C., Stöter, M., Bradshaw, C. R., Samusik, N., Rink, J. C., Kenski, D., Habermann, B., Buchholz, F., Henschel, R., Mueller, M. S. et al. (2010). Systems survey of endocytosis by multiparametric image analysis. *Nature* **464**, 243-249.

Efimov, A. and Kaverina, I. (2009). Significance of microtubule catastrophes at focal adhesion sites. *Cell Adh. Migr.* **3**, 285-287.

Erfle, H., Neumann, B., Rogers, P., Bulkescher, J., Ellenberg, J. and Pepperkok, R. (2008). Work flow for multiplexing siRNA assays by solid-phase reverse transfection in multiwell plates. *J. Biomol. Screen.* **13**, 575-580.

Etienne-Manneville, S. (2013). Microtubules in cell migration. *Annu. Rev. Cell Dev. Biol.* **29**, 471-499.

Ezratty, E. J., Partridge, M. A. and Gundersen, G. G. (2005). Microtubule-induced focal adhesion disassembly is mediated by dynamin and focal adhesion kinase. *Nat. Cell Biol.* **7**, 581-590.

Franco, S. J., Rodgers, M. A., Perrin, B. J., Han, J., Bennin, D. A., Critchley, D. R. and Huttenlocher, A. (2004). Calpain-mediated proteolysis of talin regulates adhesion dynamics. *Nat. Cell Biol.* **6**, 977-983.

Gálvez, B. G., Matías-Román, S., Albar, J. P., Sánchez-Madrid, F. and Arroyo, A. G. (2001). Membrane type 1-matrix metalloproteinase is activated during migration of human endothelial cells and modulates endothelial motility and matrix remodeling. *J. Biol. Chem.* **276**, 37491-37500.

Gauthier, N. C., Masters, T. A. and Sheetz, M. P. (2012). Mechanical feedback between membrane tension and dynamics. *Trends Cell Biol.* **22**, 527-535.

Grande-García, A., Echarri, A., de Rooij, J., Alderson, N. B., Waterman-Storer, C. M., Valdivielso, J. M. and del Pozo, M. A. (2007). Caveolin-1 regulates cell polarization and directional migration through Src kinase and Rho GTPases. *J. Cell Biol.* **177**, 683-694.

Grigoriev, I., Yu, K. L., Martinez-Sanchez, E., Serra-Marques, A., Smal, I., Meijering, E., Demmers, J., Peränen, J., Pasterkamp, R. J., van der Sluijs, P. et al. (2011). Rab6, Rab8, and MICAL3 cooperate in controlling docking and fusion of exocytotic carriers. *Curr. Biol.* **21**, 967-974.

Guo, W., Roth, D., Walch-Solimena, C. and Novick, P. (1999). The exocyst is an effector for Sec4p, targeting secretory vesicles to sites of exocytosis. *EMBO J.* **18**, 1071-1080.

Hall, A. (2012). Rho family GTPases. *Biochem. Soc. Trans.* **40**, 1378-1382.

Hamelers, I. H. L., Olivo, C., Mertens, A. E. E., Michiel Pegtel, D., van der Kammen, R. A., Sonnenberg, A. and Collard, J. G. (2005). The Rac activator Tiam1 is required for alpha3beta1-mediated laminin-5 deposition, cell spreading, and cell migration. *J. Cell Biol.* **171**, 871-881.

Hattula, K., Furuhjelm, J., Arffman, A. and Peränen, J. (2002). A Rab8-specific GDP/GTP exchange factor is involved in actin remodeling and polarized membrane transport. *Mol. Biol. Cell* **13**, 3268-3280.

Hattula, K., Furuhjelm, J., Tikkanen, J., Tanhuanpää, K., Laakkonen, P. and Peränen, J. (2006). Characterization of the Rab8-specific membrane traffic route linked to protrusion formation. *J. Cell Sci.* **119**, 4866-4877.

Henry, L. and Sheff, D. R. (2008). Rab8 Regulates Basolateral Secretory, But Not Recycling, Traffic at the Recycling Endosome. *Mol. Biol. Cell* **19**, 2059-2068.

Hopkins, C. R., Gibson, A., Shipman, M., Strickland, D. K. and Trowbridge, I. S. (1994). In migrating fibroblasts, recycling receptors are concentrated in narrow tubules in the pericentriolar area, and then routed to the plasma membrane of the leading lamella. *J. Cell Biol.* **125**, 1265-1274.

Howes, M. T., Kirkham, M., Riches, J., Cortese, K., Walser, P. J., Simpson, F., Hill, M. M., Jones, A., Lundmark, R., Lindsay, M. R. et al. (2010). Clathrin-independent carriers form a high capacity endocytic sorting system at the leading edge of migrating cells. *J. Cell Biol.* **190**, 675-691.

Huber, L. A., Pimplikar, S., Parton, R. G., Virta, H., Zerial, M. and Simons, K. (1993). Rab8, a small GTPase involved in vesicular traffic between the TGN and the basolateral plasma membrane. *J. Cell Biol.* **123**, 35-45.

Itoh, R. E., Kurokawa, K., Ohba, Y., Yoshizaki, H., Mochizuki, N. and Matsuda, M. (2002). Activation of rac and cdc42 video imaged by fluorescent resonance energy transfer-based single-molecule probes in the membrane of living cells. *Mol. Cell. Biol.* **22**, 6582-6591.

Kanerva, K., Uronen, R.-L., Blom, T., Li, S., Bittman, R., Lappalainen, P., Peränen, J., Raposo, G. and Ikonen, E. (2013). LDL cholesterol recycles to the plasma membrane via a Rab8a-Myosin5b-actin-dependent membrane transport route. *Dev. Cell* **27**, 249-262.

Kaverina, I., Krylyshkina, O. and Small, J. V. (1999). Microtubule targeting of substrate contacts promotes their relaxation and dissociation. *J. Cell Biol.* **146**, 1033-1044.

Khandelwal, P., Prakasam, H. S., Clayton, D. R., Ruiz, W. G., Gallo, L. I., van Roekel, D., Lukianov, S., Peränen, J., Goldenring, J. R. and Apodaca, G. (2013). A Rab11a-Rab8a-Myo5B network promotes stretch-regulated exocytosis in bladder umbrella cells. *Mol. Biol. Cell* **24**, 1007-1019.

Lansbergen, G., Grigoriev, I., Mimori-Kiyosue, Y., Ohtsuka, T., Higa, S., Kitajima, I., Demmers, J., Galjart, N., Houtsmuller, A. B., Grosveld, F. et al. (2006). CLASPs attach microtubule plus ends to the cell cortex through a complex with LL5β *Dev. Cell* **11**, 21-32.

Letinic, K., Sebastian, R., Toomre, D. and Rakic, P. (2009). Exocyst is involved in polarized cell migration and cerebral cortical development. *Proc. Natl. Acad. Sci. USA* **106**, 11342-11347.

Liu, J., Yue, P., Artym, V. V., Mueller, S. C. and Guo, W. (2009). The role of the exocyst in matrix metalloproteinase secretion and actin dynamics during tumor cell invadopodia formation. *Mol. Biol. Cell* **20**, 3763-3771.

Megías, D., Marrero, R., del Peso, B. M., García, M. Á., Bravo-Cordero, J.-J., García-Grande, A., Santos, A. and Montoya, M. C. (2009). Novel lambda FRET spectral confocal microscopy imaging method. *Microsc. Res. Tech.* **72**, 1-11.

Monteiro, P., Rossé, C., Castro-Castro, A., Irondelle, M., Lagoutte, E., Paul-Gilloteaux, P., Desnos, C., Formstecher, E., Darchen, F., Perrais, D. et al. (2013). Endosomal WASH and exocyst complexes control exocytosis of MT1-MMP at invadopodia. *J. Cell Biol.* **203**, 1063-1079.

Navarro-Lérida, I., Sánchez-Perales, S., Calvo, M., Rentero, C., Zheng, Y., Enrich, C. and Del Pozo, M. A. (2012). A palmitoylation switch mechanism regulates Rac1 function and membrane organization. *EMBO J.* **31**, 534-551.

Osmani, N., Peglion, F., Chavrier, P. and Etienne-Manneville, S. (2010). Cdc42 localization and cell polarity depend on membrane traffic. *J. Cell Biol.* **191**, 1261-1269.

Palamidessi, A., Frittoli, E., Garré, M., Faretta, M., Mione, M., Testa, I., Diaspro, A., Lanzetti, L., Scita, G., Di Fiore, P. P. et al. (2008). Endocytic trafficking of Rac is required for the spatial restriction of signaling in cell migration. *Cell* **134**, 135-147.

Pankov, R., Endo, Y., Even-Ram, S., Araki, M., Clark, K., Cukierman, E., Matsumoto, K. and Yamada, K. M. (2005). A Rac switch regulates random versus directionally persistent cell migration. *J. Cell Biol.* **170**, 793-802.

Pathak, R., Delorme-walker, V. D., Howell, M. C., Anselmo, A. N., White, M. A., Bokoch, G. M. and Dermardirossian, C. (2013). The microtubule-associated Rho activating factor GEF-H1 interacts with Exocyst complex to regulate Vesicle Traffic. *Dev. Cell* **23**, 397-411.

Peränen, J., Auvinen, P., Virta, H., Wepf, R. and Simons, K. (1996). Rab8 promotes polarized membrane transport through reorganization of actin and microtubules in fibroblasts. *J. Cell Biol.* **135**, 153-167.

Powelka, A. M., Sun, J., Li, J., Gao, M., Shaw, L. M., Sonnenberg, A. and Hsu, V. W. (2004). Stimulation-dependent recycling of integrin beta1 regulated by ARF6 and Rab11. *Traffic* **5**, 20-36.

Prigozhina, N. L. and Waterman-Storer, C. M. (2006). Decreased polarity and increased random motility in PtK1 epithelial cells correlate with inhibition of endosomal recycling. *J. Cell Sci.* **119**, 3571-3582.

Roland, J. T., Kenworthy, A. K., Peranen, J., Caplan, S. and Goldenring, J. R. (2007). Myosin Vb interacts with Rab8a on a tubular network containing EHD1 and EHD3. *Mol. Biol. Cell* **18**, 2828-2837.

Rooney, C., White, G., Nazgiewicz, A., Woodcock, S. A., Anderson, K. I., Ballestrem, C. and Malliri, A. (2010). The Rac activator STEF (Tiam2) regulates cell migration by microtubule-mediated focal adhesion disassembly. *EMBO Rep.* **11**, 292-298.

Sakurai-Yageta, M., Recchi, C., Le Dez, G., Sibarita, J.-B., Daviet, L., Camonis, J., D'Souza-Schorey, C. and Chavrier, P. (2008). The interaction of IQGAP1 with the exocyst complex is required for tumor cell invasion downstream of Cdc42 and RhoA. *J. Cell Biol.* **181**, 985-998.

Schmoranzer, J., Kreitzer, G. and Simon, S. M. (2003). Migrating fibroblasts perform polarized, microtubule-dependent exocytosis towards the leading edge. *J. Cell Sci.* **116**, 4513-4519.

Small, J. V. and Kaverina, I. (2003). Microtubules meet substrate adhesions to arrange cell polarity. *Curr. Opin. Cell Biol.* **15**, 40-47.

Spiczka, K. S. and Yeaman, C. (2008). Ral-regulated interaction between Sec5 and paxillin targets Exocyst to focal complexes during cell migration. *J. Cell Sci.* **121**, 2880-2891.

Steffen, A., Le Dez, G., Poincloux, R., Recchi, C., Nassoy, P., Rottner, K., Galli, T. and Chavrier, P. (2008). MT1-MMP-dependent invasion is regulated by TI-VAMP/VAMP7. *Curr. Biol.* **18**, 926-931.

Stehbens, S. and Wittmann, T. (2012). Targeting and transport: how microtubules control focal adhesion dynamics. *J. Cell Biol.* **198**, 481-489.

Stehbens, S. J., Paszek, M., Pemble, H., Ettinger, A., Gierke, S. and Wittmann, T. (2014). CLASPs link focal-adhesion-associated microtubule capture to localized exocytosis and adhesion site turnover. *Nat. Cell Biol.* **16**, 561-573.

Sun, Y., Chiu, T. T., Foley, K. P., Bilan, P. J. and Klip, A. (2014). Myosin Va mediates Rab8A-regulated GLUT4 vesicle exocytosis in insulin-stimulated muscle cells. *Mol. Biol. Cell* **25**, 1159-1170.

Takino, T., Watanabe, Y., Matsui, M., Miyamori, H., Kudo, T., Seiki, M. and Sato, H. (2006). Membrane-type 1 matrix metalloproteinase modulates focal adhesion stability and cell migration. *Exp. Cell Res.* **312**, 1381-1389.

Wang, Y. and McNiven, M. A. (2012). Invasive matrix degradation at focal adhesions occurs via protease recruitment by a FAK–p130Cas complex. *J. Cell Biol.* **196**, 375-385.

Wang, J., Ren, J., Wu, B., Feng, S., Cai, G., Tuluc, F., Peränen, J. and Guo, W. (2015). Activation of Rab8 guanine nucleotide exchange factor Rabin8 by ERK1/2 in response to EGF signaling. *Proc. Natl. Acad. Sci. USA* **112**, 148-153.

White, D. P., Caswell, P. T. and Norman, J. C. (2007). alpha v beta3 and alpha5beta1 integrin recycling pathways dictate downstream Rho kinase signaling to regulate persistent cell migration. *J. Cell Biol.* **177**, 515-525.

Wiesner, C., El Azzouzi, K. and Linder, S. (2013). A specific subset of RabGTPases controls cell surface exposure of MT1-MMP, extracellular matrix degradation and three-dimensional invasion of macrophages. *J. Cell Sci.* **126**, 2820-2833.

Williams, K. C. and Coppolino, M. G. (2011). Phosphorylation of membrane type 1-matrix metalloproteinase (MT1-MMP) and its vesicle-associated membrane protein 7 (VAMP7)-dependent trafficking facilitate cell invasion and migration. *J. Biol. Chem.* **286**, 43405-43416.

Yamamura, R., Nishimura, N., Nakatsuji, H., Arase, S. and Sasaki, T. (2008). The interaction of JRAB/MICAL-L2 with Rab8 and Rab13 coordinates the assembly of tight junctions and adherens junctions. *Mol. Biol. Cell* **19**, 971-983.